Metal-Based Paullones as Putative CDK Inhibitors for Antitumor Chemotherapy

Wolfgang F. Schmid,[†] Roland O. John,[†] Gerhard Mühlgassner,[†] Petra Heffeter,[‡] Michael A. Jakupec,[†] Markus Galanski,[†] Walter Berger,[‡] Vladimir B. Arion,*[,†] and Bernhard K. Keppler*[,†]

Institute of Inorganic Chemistry, University of Vienna, Währingerstr. 42, A-1090 Vienna, Austria, and Institute of Cancer Research, Medical University of Vienna, Borschkegasse 8a, A-1090 Vienna, Austria

Received August 22, 2007

Paullones constitute a class of potent cyclin-dependent kinase inhibitors. To overcome the insufficient solubility and bioavailability, which hamper their potential medical application, we aim at the development of metal-based derivatives. Two types of paullone ligands, $\mathbf{L^1}$–$\mathbf{L^3}$ and $\mathbf{L^4}$, with different locations of metal-binding sites, were prepared. They were found to form organometallic complexes of the general formula $[M^{II}Cl(\eta^6$-*p*-cymene)L]Cl (**1**–**4**, L = $\mathbf{L^1}$–$\mathbf{L^4}$; **a**, M = Ru; **b**, M = Os). The complexes were characterized by X-ray crystallography, one- and two-dimensional NMR spectroscopy and other physical methods. Complexes **1**–**3**, with a coordinated amidine unit, were found to undergo *E*/*Z* isomerization in solution. The reaction was studied by NMR spectroscopy, and activation parameters $\Delta H^{\ddagger}$ and $\Delta S^{\ddagger}$ were determined. Antiproliferative activity in the low micromolar range was observed *in vitro* in three human cancer cell lines by means of MTT assays. ^{3}H-Thymidine incorporation assays revealed the compounds to lower the rate of DNA synthesis, and flow cytometric analyses showed cell cycle arrest mainly in G_0/G_1 phase.

Introduction

Organometallic ruthenium(II) arene complexes with antiproliferative activity *in vitro* are extensively being studied as potential novel anticancer drugs.[1–3] Their reactivity toward nucleobases and DNA was found to be similar to cisplatin,[4–6] and structure−cytotoxicity relationships have been elucidated.[7] So far, only a few reports have been published on arene complexes of the heavier congener osmium(II), which show cytotoxicity in cancer cells.[8–10]

Arene complexes provide an ideal metal scaffold to deliver antitumor compounds to tumor cells, because they combine a proper lipophilicity for transport through cell membranes with a relatively high aqueous solubility and stabilize ruthenium(II).[11] The effect of binding of organic compounds to organometallic moieties on their biological activity has been documented in the literature.[12–17] In these particular cases, complexation endowed the employed biologically relevant ligands with higher affinity toward their targets, increased solubility, increased cellular uptake, higher accumulation in the cell nucleus, the capability of DNA interactions, and the propensity to overcome acquired resistance to the metal-free drugs.

A family of dihydroindolobenzazepines, the paullones (Chart 1),[18] was discovered as potent inhibitors[19] of cyclin-dependent kinases (CDKs[a]), which control cell cycle progression[20] and show increased activity in cancer cells due to upregulated cyclin expression. This makes the paullones interesting candidates for the development of targeted antitumor drugs. An underivatized lactam unit is essential for CDK inhibition for steric complementarity reasons, and electron-withdrawing substituents in position 9 increase CDK inhibitory activity.[21] Because the antiproliferative activity of a number of paullones does not parallel their CDK inhibitory potency, other intracellular targets have also been considered: 9-nitro paullone (alsterpaullone) was discovered to possess considerable affinity to glycogen synthase kinase (GSK-3) and mitochondrial malate dehydrogenase (mMDH).[22] Moreover, a lactam-substituted paullone was shown quite recently to inhibit sirtuins (SIRT; NAD^+-dependent deacetylases), which are likely linked to the pathogenesis of viral diseases and cancer.[23] Independent studies on alsterpaullone and on the antitumor ruthenium(III) complex $(H_2ind)[trans$-$Ru^{III}Cl_4(Hind)_2]$ (KP1019; Hind = indazole),[24] which is probably activated by reduction to ruthenium(II),[25] showed both to be able to induce apoptosis through the intrinsic mitochondrial pathway.[26,27]

However, paullones have limited water solubility, which makes on the one hand the antiproliferative screening difficult and on the other hand reduces the bioavailability of the potential drugs in the human body. As a part of a larger project in which structure−cytotoxicity relationships of a series of structurally varied paullones are investigated, we attempted to design paullones able to bind to metal ions and especially to the ruthenium(II) and osmium(II) arene moiety. We anticipated that coordination of neutral paullone derivatives will result in ionic compounds with increased aqueous solubility as compared to metal-free paullones and neutral ruthenium(II) paullone coordination compounds,[28] enabling assays of their biological activity and elucidation of a number of novel aspects of their chemical and biological behavior.

We report herein the synthesis and characterization of paullones with a different location of the metal-binding site and their ruthenium(II) and osmium(II) arene complexes. This synthetic success enabled the study of the effect of (i) substitution of ruthenium(II) by osmium(II), (ii) variation of substituents at position 9 of the paullone framework, and (iii) the location of the metalation site on the electronic, structural, antiproliferative, and cell cycle arresting properties of these compounds and their behavior in solution. Our data suggest that metal-based paullone derivatives are potential candidates

* To whom correspondence should be addressed. Phone: +43 1 4277 52680 (V.B.A.); +43 1 4277 52600 (B.K.K.). Fax: +43 1 4277 52630 (V.B.A.); +43 1 4277 52680 (B.K.K.). E-mail: vladimir.arion@univie.ac.at (V.B.A.); bernhard.keppler@univie.ac.at (B.K.K.).

[†] University of Vienna.

[‡] Medical University of Vienna.

[a] Abbreviations: CDK, cyclin-dependent kinase; MTT, 3-(4,5-dimethylthiazol-2-yl)-2,5-diphenyltetrazolium bromide; ANOVA, analysis of variance; NOE, nuclear Overhauser effect.

10.1021/jm701042w CCC: $37.00
Published on Web 11/13/2007

Chart 1. Structure of Paullones with Atom Numbering Scheme

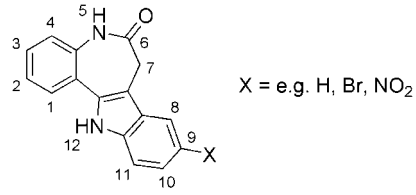

for further development and medical applications as antitumor chemotherapeutics.

Results

Synthesis and Characterization of Ligands and Complexes. Two types of paullone ligands, $\mathbf{L^1}$–$\mathbf{L^3}$ and $\mathbf{L^4}$, and eight novel complexes of the general formula $[M^{II}Cl(\eta^6\text{-}p\text{-cymene})L]^+$ (**1**–**4**, L = $\mathbf{L^1}$–$\mathbf{L^4}$; **a**, M = Ru, **b**, M = Os) have been prepared in good yields, as shown in Scheme 1.

As expected, all neutral paullone ligands were bound to the organometallic moieties in a bidentate fashion, rendering the complexes monocationic. A common method to isolate such complexes is their precipitation as hexafluorophosphates. Instead, we found conditions for the crystallization of these compounds as chlorides. All prepared compounds were characterized by IR and UV–vis spectroscopy and conductivity measurements (see Supporting Information).

Cyclic voltammograms showed irreversible, presumably ligand-centered, reduction bands at $E_{p/2} = -1.0$, -1.38, -0.58, and -0.61 V for **1a**, **1b**, **4a**, and **4b**, correspondingly (Figure S8). The species formed upon reduction were oxidized at $E_{p/2} = -0.21$ and -0.19 V in the cases of **4a** and **4b** only. The metal-free ligands were electrochemically silent between –1.5 and +1.0 V.

Crystal Structures. The results of X-ray diffraction studies of $\mathbf{L^3}$, the *Z*-isomers of **1b** and **2b**, the *E*- and *Z*-isomers of **3a**, the *E*-isomer of **3b**, and of the complexes **4a** and **4b** are displayed in Figures S1, 1, S2, 2, S3, S4, and 3, correspondingly. All complexes adopt the familiar "three-leg piano stool" geometry, with the nitrogen atoms of the picolylamine (**1**–**3**) or picolylenamine (**4a**, **4b**) moiety and the chloro ligand as the legs of the piano stool and the arene ligand as the seat.

The use of unsymmetrical N−N paullone ligands induces chirality at the metal centers (ruthenium or osmium). Ranking the ligating atoms and molecules in the crystal structure of *Z*-**1b** in accord with the priority rules[29,30] (arene > Cl1/Cl2 > N3/N7 > N4/N8) and applying the skew-lines convention[31] to the chelate ring, we define the first and second crystallographically independent cations to form the enantiomeric pair $S_O,\delta/R_O,\lambda$. In addition, the configuration adopted by the paullone ligands $\mathbf{L^1}$−$\mathbf{L^3}$ is described as *E* or *Z* in dependence of the location of the methylene group of the picolylamine moiety and the nitrogen atom of the seven-membered azepine ring relative to the double bond joining the picolylamine residue with the seven-membered azepine ring (that is, C12−N3 in the first and C44−N7 in the second independent cation of *Z*-**1b** in Figure 1). Because in the chelate rings in **4a** and **4b** are planar, no δ/λ chirality is induced. All complexes **1**–**4**, except *Z*-**1b**, were found to have their cymene ligand oriented with its isopropyl group above the chelate ring. Crystallographic data and details of data collection are given in Table S1, and selected bond distances and angles are in Table S2 and in the legends to Figures 1, 3, S1, S2, and S4.

^{1}H NMR Spectra. ^{1}H NMR spectra of $\mathbf{L^3}$ in DMSO-d_6 closely resemble those of $\mathbf{L^1}$ and $\mathbf{L^2}$,[28] because they only differ in the substituent in position 9 of the paullone scaffold (Chart 2). These three paullone ligands adopt a configuration with endocyclic double bond $C^6{=}N^5$ in solution, as evidenced by the doublet of the methylene protons H^{14} of the α-picolylamine moiety at 4.5 ppm and the triplet of the amidine nitrogen proton H^{13} at 7.8 ($\mathbf{L^1}$, $\mathbf{L^2}$) or 7.9 ppm ($\mathbf{L^3}$). In $\mathbf{L^4}$, the azepine lactam unit is not functionalized, displaying H^5 at 10.1 ppm. For all four ligands, the azepine methylene protons H^7 are found at 3.4 ($\mathbf{L^1}$, $\mathbf{L^2}$), 3.5 ($\mathbf{L^3}$), or at 3.6 ppm ($\mathbf{L^4}$) as a singlet, in accord with fast inversion of the seven-membered azepine ring.

Upon coordination to ruthenium or osmium, the amidine NH proton resonance of $\mathbf{L^1}$, $\mathbf{L^2}$, or $\mathbf{L^3}$ is downfield-shifted by 1.0 to 2.2 ppm. In addition, it appears as a singlet as the result of the ligand rearrangement to the configuration with exocyclic double bond $C^6{=}N^{13}$, with the amidine nitrogen atom N^5 being protonated instead of N^{13}. The methylene groups of the α-picolylamine moiety and the azepine methylene group show diastereotopic splitting in these complexes. In contrast, $\mathbf{L^4}$ displays its H^7 resonance as a singlet also in its complexes **4a** and **4b**.

***E*/*Z* Isomerization Behavior of 1–3.** In the ^{1}H NMR spectra of complexes **1**–**3** in DMSO-d_6, measured immediately after dissolution, two signal sets of different relative intensities were observed. Repeated acquisition of NMR spectra revealed the prevailing signal set to decrease with time, while the second, less intense signal set increased until equilibrium was reached. The amount of the second, accumulating species never reached that of the declining species in dimethyl sulfoxide (Figure S10). In particular, the relative intensities of the first and second signal set for **1a** changed from 54.6:1 immediately after dissolution to 1.4:1 at equilibrium. However, this equilibrium was found to be solvent-dependent. In methanol-d_4, the relative intensities of the two signal sets for **1a** changed from 61.5:1 immediately after dissolution to 1:11 at equilibrium.

Because both signal sets differed markedly from those observed for the corresponding ligands, a complexation−decomplexation equilibrium was excluded (Figure S10). In addition, the observed time-dependent changes for **3a** were not affected by the presence of an excess of chloride ions in methanol, providing evidence against solvolysis of the Ru−Cl bond. In line with these data were also the ESI mass spectra of the same compound, which showed the presence of peaks at *m*/*z* 654 and 618, attributed to $[RuCl(cymene)\mathbf{L^3}]^+$ and $[RuCl(cymene)\mathbf{L^3} - HCl]^+$, while no other peaks were observed when a methanol solution of the complexes, which had reached equilibrium, was used for measurements.

X-ray diffraction study of **2b** revealed the ligand to adopt the *Z*-configuration at the exocyclic amidine double bond $C^6{=}N^{13}$, in contrast to **3a** and **3b** and ruthenium(II) paullone coordination compounds,[28] in which the ligands were found to be the *E*-isomers. Upon careful examination of the crystals obtained from a synthesis of **3a**, we found two types, that is, blocks and sticks. Both were big enough for separation under a microscope. Subsequent NMR study of both isolated fractions showed that each of them can be characterized by one set of the previously observed signals (Figure 4). Starting from separated species, the same equilibrium ratio was achieved in solution (Figure 5). Gratifyingly, both types of separated crystals proved to be suitable for X-ray diffraction studies, which revealed the presence of two different isomers for **3a**: *E* (block-shaped crystals, Figure 2A) and *Z* (stick-shaped crystals, Figure 2B). These results provided unequivocal evidence for an *E*/*Z* isomerization process at the exocyclic amidine $C^6{=}N^{13}$ bond in solutions of **1**–**3**. The results of kinetic ^{1}H NMR studies on

Scheme 1. Synthesis of Ligands and Complexes

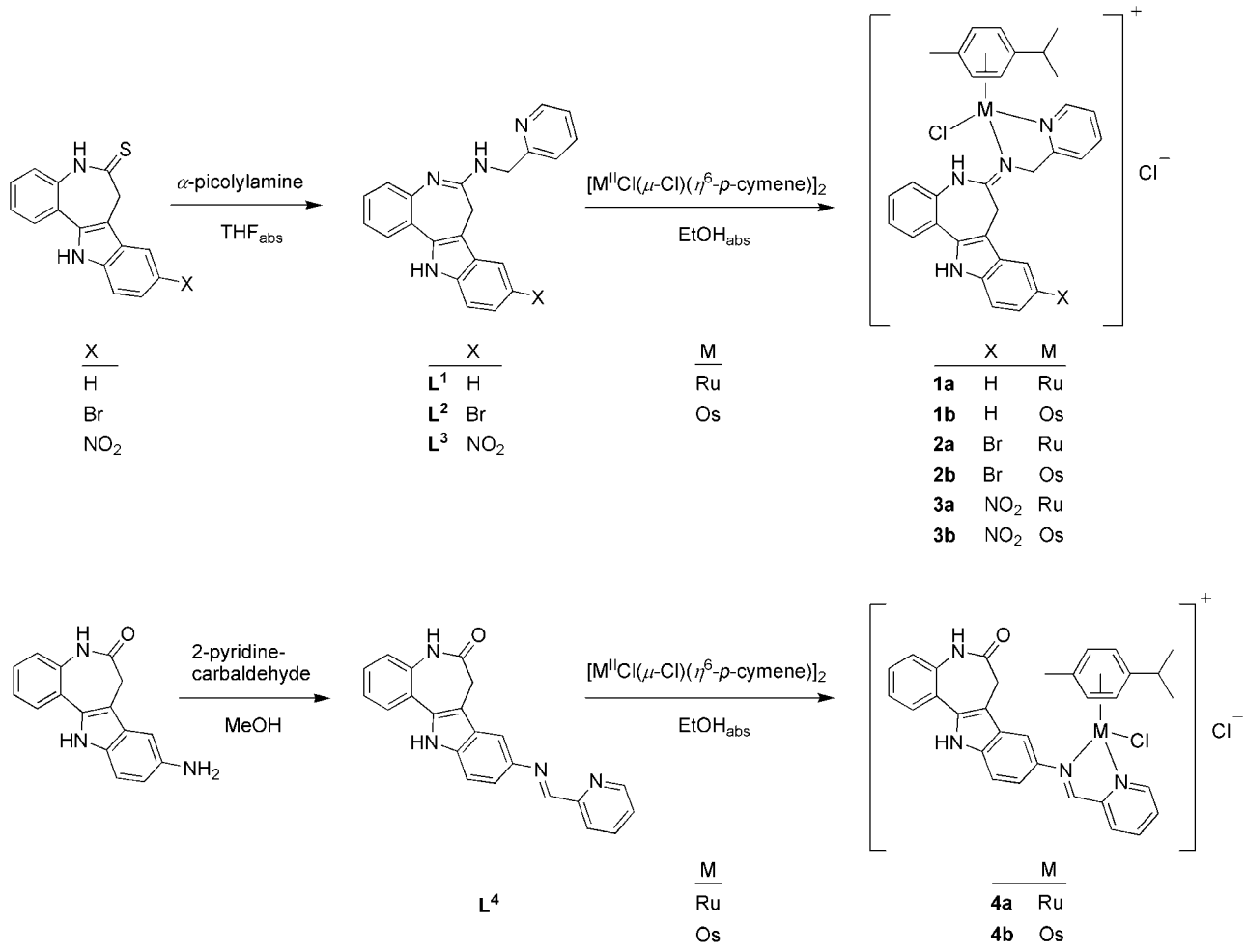

X
H
Br
NO_2

	X
L^1	H
L^2	Br
L^3	NO_2

M
Ru
Os

	X	M
1a	H	Ru
1b	H	Os
2a	Br	Ru
2b	Br	Os
3a	NO_2	Ru
3b	NO_2	Os

L^4

M
Ru
Os

	M
4a	Ru
4b	Os

the *E*/*Z* isomerization of **1**–**3** are summarized in Tables 1 and 2 and Figure 6.

Analysis of the bulk samples obtained from complexation of **L^1**, **L^2**, and **L^3** with ruthenium(II) and osmium(II) arene precursors indicated that generally a mixture of *E*/*Z* isomers is prepared, in which the stick-shaped crystals of the *Z*-isomer dominate over the block-shaped crystals of the *E*-isomer.

For the *E*/*Z* isomerization of **3a**, activation parameters were determined using the Eyring equation by carrying out experiments at 24, 40, 50, and 60 °C starting from the *Z*-isomer (Figure 7). Errors were estimated from two fits with minimal and maximal slope. The partial reaction $Z \rightarrow E$ was found to possess $\Delta H^{\ddagger}_{ZE} = 110.6 \pm 0.9$ kJ/mol and $\Delta S^{\ddagger}_{ZE} = 87.8 \pm 3.2$ J/(K mol), while for the partial reaction $E \rightarrow Z$, the corresponding parameters were found to be $\Delta H^{\ddagger}_{EZ} = 99.8 \pm 1.0$ kJ/mol and $\Delta S^{\ddagger}_{EZ} = 59.7 \pm 3.4$ J/(K mol).

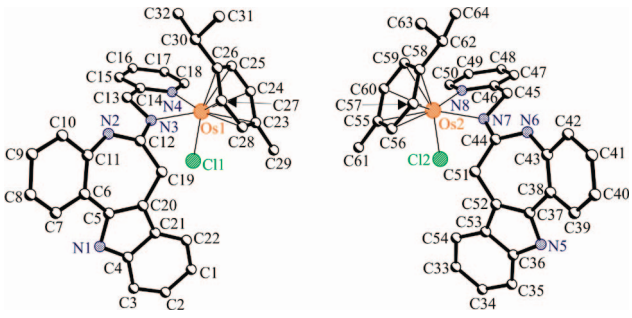

Figure 1. X-ray structures of both independent cations of *Z*-**1b** with atom numbering schemes. H atoms have been omitted for clarity. Selected bond distances (Å) and angles (°): Os1−arene ring centroid 1.664, Os2−arene ring centroid 1.662, Os1−N3 2.124(8), Os2−N7 2.121(9), Os1−N4 2.081(9), Os2−N8 2.100(9), Os1−Cl1 2.408(3), Os2−Cl2 2.405(3), N2−C12 1.357(13), N6−C44 1.370(12), C12−N3 1.316(13), C44−N7 1.278(13), N3−Os1−N4 77.1(4), N7−Os2−N8 77.5(3), $\Theta_{N3\text{-}C13\text{-}C14\text{-}N4}$ −19.9(13), $\Theta_{N7\text{-}C45\text{-}C46\text{-}N8}$ 26.0(13), $\Theta_{N1\text{-}C5\text{-}C6\text{-}C7}$ 18(2), $\Theta_{N5\text{-}C37\text{-}C38\text{-}C39}$ −28.1(17).

Studies of Hydrolysis and Reactivity Toward 5′-GMP. Solutions of all complexes and ligands in H_2O/DMSO = 95:5 were analyzed by UV–vis spectroscopy to judge the stability of the compounds. Only minor spectral changes were observed over 72 h (Figures S5 and S6). Together with ^{1}H NMR spectra in this solvent mixture, this indicates only partial hydrolysis of M−Cl bonds.

The hydrolysis behavior of **1a**, **1b**, **4a**, and **4b** was also studied by ^{1}H NMR spectroscopy in D_2O/DMSO-d_6 = 90:10. Complexes **1a** and **1b** formed two additional species that were attributed to the aqua complexes with *E*- and *Z*-configuration at the exocyclic amidine double bond. This assignment was supported by the observation that their amount was reduced significantly if 4 equiv NaCl were present and that they could also be formed immediately upon addition of silver nitrate. After 72 h, the ratio chloro-*E*/chloro-*Z*/aqua-*E*/aqua-*Z* was found to be 58:18:8:16 without and 68:24:3:5 with 4 equiv NaCl for **1a** and 60:27:5:8 without and 61:32:3:4 with 4 equiv NaCl for **1b**. The extent of hydrolysis of the osmium complex is thus reduced to about half that of the ruthenium complex if no additional chloride ions are present, while it is similarly low for both in

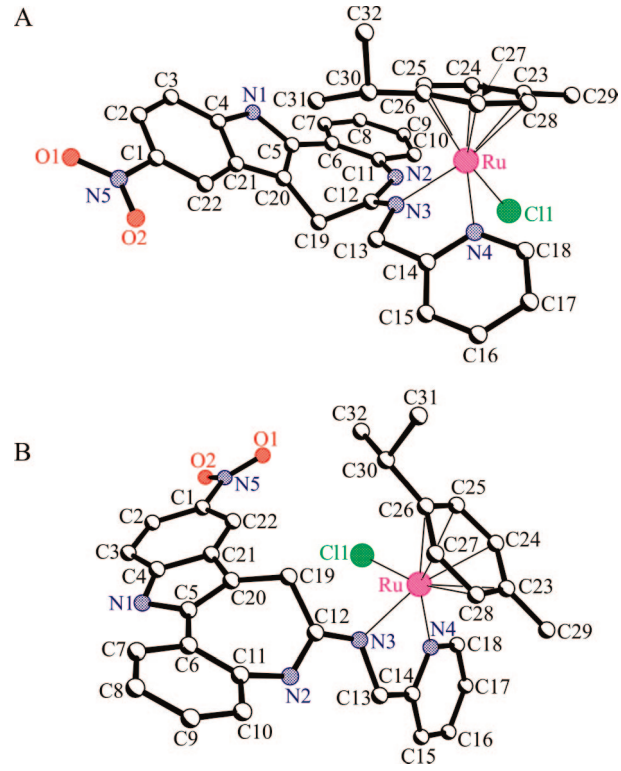

Figure 2. X-ray structures of the cations of (A) *E*-**3a** and (B) *Z*-**3a** with atom numbering schemes. H atoms have been omitted for clarity. Selected bond distances and angles are given in Table S2.

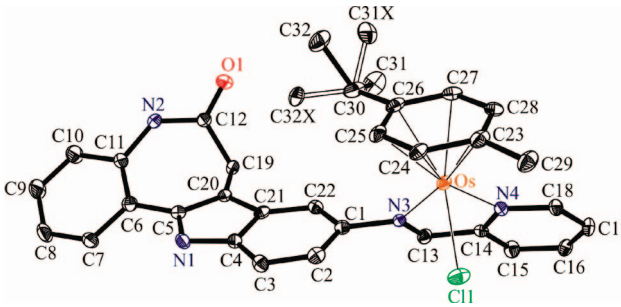

Figure 3. ORTEP view of the structure of the cation of **4b** with atom numbering scheme. Thermal ellipsoids are drawn at the 50% probability level. H atoms have been omitted for clarity. The isopropyl methyl groups of the arene ligand are disordered over two positions with occupancies of 70 and 30%, respectively. Selected bond distances (Å) and angles (°): Os1−arene ring centroid 1.686, Os1−N3 2.091(3), Os1−N4 2.080(3), Os1−Cl1 2.3820(10), C1−N3 1.445(5), N3−C13 1.288(5), C13−C14 1.452(5), N3−Os1−N4 75.58(12), $\Theta_{N3\text{-}C13\text{-}C14\text{-}N4}$ −0.5(5), $\Theta_{C13\text{-}N3\text{-}C1\text{-}C2}$ 125.8(4), $\Theta_{N1\text{-}C5\text{-}C6\text{-}C7}$ −29.3(5).

the presence of 4 equiv NaCl. For **4a** and **4b**, the ratio between the chloro and aqua complexes after 72 h was determined as 74:26 and 87:13, respectively, which closely resembles the sums of chloro and aqua complexes observed for **1a** and **1b**. The formation of hydroxo-bridged dimers[35] was observed in neither case.

For the aqua complexes of *E*-**1a** and *E*-**1b**, the pK_a* values were determined as 7.35 and 6.17 by ^{1}H NMR titration studies (Figure 8), while those of the corresponding *Z*-isomers are higher, but could not be determined because of complete isomerization to the *E*-isomers at pH* > 9 (**1a**) and >8 (**1b**).

The reactivity of **1a** and **4a** toward 5′-GMP in equimolar ratio at 37 °C was analyzed by means of ^{1}H and ^{31}P NMR spectroscopy. Individual solutions of **1a**, **4a**, and 5′-GMP were used as negative controls. After 72 h of monitoring, the content of two new species attributable to formed 5′-GMP complexes in the spectra of **1a** and **4a** could be estimated by integration of the emerged ^{31}P signals to be about 10% only. The corresponding aqua complexes, generated by the addition of silver nitrate and filtering off silver chloride, showed a similar reaction profile.

Cytotoxicity. The ruthenium and osmium complexes were tested by means of the colorimetric MTT assay for their antiproliferative activity in three human tumor cell lines: A549 (non-small cell lung carcinoma), CH1 (ovarian carcinoma), and SW480 (colon carcinoma). These are derived from common forms of cancer that are routinely treated with metal-based chemotherapeutic drugs in the clinical setting. Concentration−effect curves obtained after 96 h exposure are depicted in Figures 9 and 10, and IC_{50} values are listed in Table 3.

All complexes showed antiproliferative activities with IC_{50} values in a range of low micromolar concentrations, reasonable for antitumor compounds, in all three cell lines.

^{3}H-Thymidine Incorporation Assay. To investigate whether the new compounds have effects on the cell cycle comparable to CDK inhibitors, the ruthenium complexes **1a** and **4a** and the osmium complexes **1b** and **4b** were used. In a first approach, the effects of the compounds on DNA synthesis were determined by ^{3}H-thymidine incorporation assays. All four compounds significantly ($p < 0.01$ compared to control, calculated by one-way ANOVA and Dunnet test) inhibited ^{3}H-thymidine incorporation in DNA of A549 lung cancer cells (Figure 11). Comparable to the results obtained in MTT assays, **1a** and **1b** were more effective in arresting DNA synthesis than complexes **4a** and **4b**. As expected, the known CDK inhibitor staurosporine (Stau), used as a positive control in all experiments, potently arrested DNA synthesis of A549 cells.

Cell Cycle Analysis. To clarify whether the four complexes have the potential to alter the cell cycle progression, cell cycle distributions of exponentially growing A549 cells after 24 h exposure were evaluated. Comparable to staurosporine, all tested compounds led to an increase of the cell fraction in G_0/G_1 phase (Figure 12A). Overall, the complexes **1a** and **1b** displayed stronger activity and **4b** an intermediate activity, indicated by a shift in cell cycle distribution already at 20 μM, while **4a** had only a slight impact up to 50 μM (Figure 12B). Moreover, treatment with concentrations higher than 40 μM of **1a** or **1b** led to a reduction of G_0/G_1 arrest, accompanied by an increase of the apoptotic cell population. This suggests that these compounds affect cell cycle distribution only in concentrations with low cytotoxicity, while further increase of the concentration leads to apoptotic cell death.

Discussion

Synthesis. Although the number of paullone compounds is large,[21,52] there are only a few metal-based derivatives documented so far.[28,32] This is primarily because paullone species do not contain suitable metal-chelating sites. Their binding to metal ions could only be expected via lactam or thiolactam units, with the formation of thermodynamically unfavored four-membered chelate cycles. By chemical modifications of the thiolactam moiety and the amino group in position 9 of the original paullones (Chart 1), we prepared novel paullone ligands with different locations of potential binding sites capable of binding to organometallic ruthenium(II) and osmium(II) moieties.

Crystal Structures. The crystal structures of ruthenium and osmium arene complexes with paullone derivatives are the first to be reported.[33] The osmium-arene centroid distances of 1.664 and 1.662 Å in the first and second independent cation of *Z*-**1b**

Chart 2. NMR Atom Numbering Scheme and Cymene Orientations

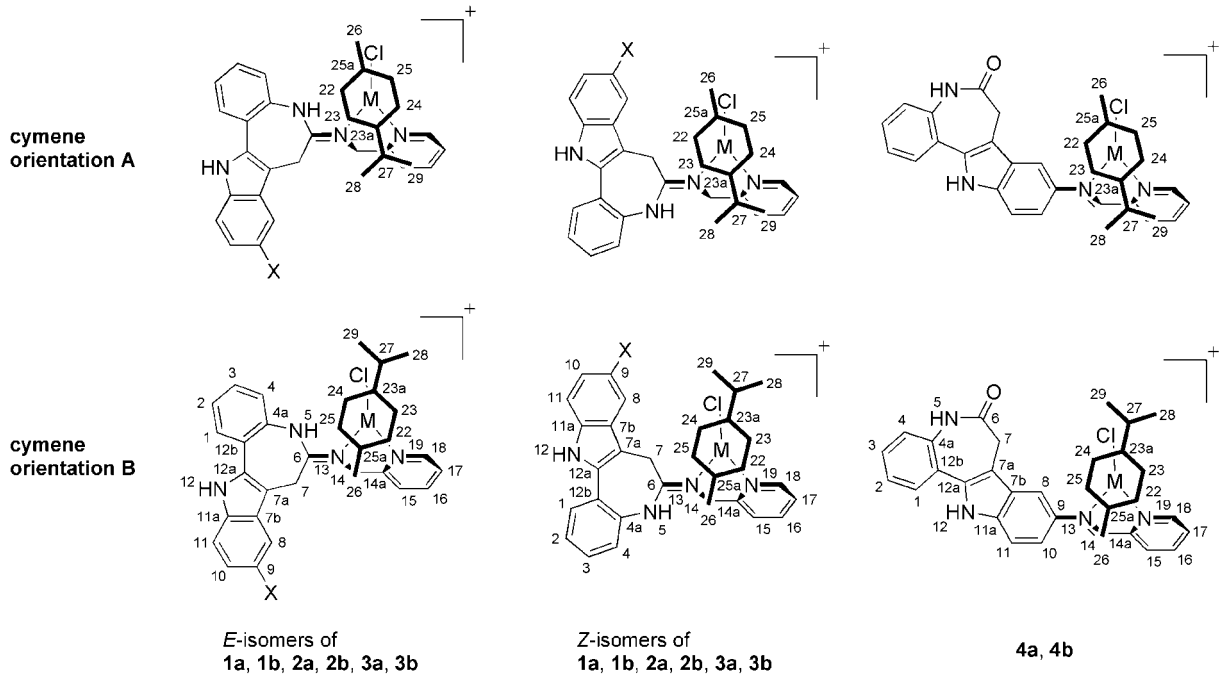

are comparable to those of analogous arene complexes, for example, 1.698 Å in [RuCl(cymene)(diimine)]PF_6[34] and 1.660 Å in [OsCl(biphenyl)(en)]BPh_4.[35] The bond lengths Os1−N3 and Os2−N7 of 2.124(8) and 2.121(9) Å are comparable to those in [OsCl(biphenyl)(en)]BPh_4[35] of 2.148(3) and 2.131(3) Å, whereas Os1−N4 and Os2−N8 of 2.081(9) and 2.100(9) Å are significantly shorter[36] and more closely resemble those in [RuCl(cymene)(diimine)]PF_6[34] of 2.080(3) and 2.103(3) Å. The bonding distances Os1−Cl1 and Os2−Cl2 of 2.408(3) and 2.405(3) Å are very similar to that in [OsCl(biphenyl)(en)]BPh_4[35] of 2.4015(9) Å.

The distribution of electron density over the coordinated paullone ligand **L**[1] is different from that in the metal-free paullone. Upon coordination, another tautomeric form of the organic ligand is stabilized. The bond N2−C12 of 1.2968(13) Å, which is significantly shorter than C12−N3 of 1.3452(14) Å in the metal-free ligand, becomes markedly longer when the paullone ligand is bound to osmium(II) [N2−C12 1.357(13) and C12−N3 1.316(13) Å]. This tendency is even more pronounced in the second independent cation of **1b** [N6−C44 1.370(12) and C44−N7 1.278(13) Å].

The ruthenium(II) complex [RuCl(cymene)**L**[3]]Cl crystallized with the paullone ligand in both configurations *E* and *Z*, suggesting that the energetic difference between these two assemblies is small enough to allow the conversion. The adopted ligand configuration only slightly affects the coordination geometry around the ruthenium atom. The bond lengths Ru1−Cl1 at 2.4015(5) and 2.3931(10) in *E*- and *Z*-**3a** are in both cases similar to that observed in [RuCl(cymene)(diimine)]PF_6[34] of 2.3964(9) Å. Although the differences are not very pronounced, the angles Cl1−M−N3 and M−N3−C12 are smaller in the *E*-isomers, which is probably due to intramolecular hydrogen bonding N2−H20···Cl1 [N2···Cl1 3.213 (*E*-**3a**) and 3.242 Å (*E*-**3b**)].[37]

The complexes [M^{II}Cl(cymene)(**L**[4])]Cl·$(CH_3)_2CO$, with M = Ru (**4a**) and Os (**4b**), are isostructural and possess common M−N3, M−N4, M−Cl1, and M−arene centroid distances[34,35]

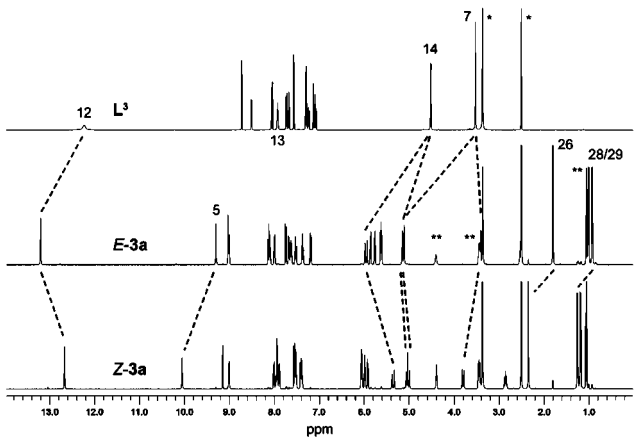

Figure 4. [1]H NMR spectra of **L**[3] (upper trace), [RuCl(cymene)(*E*-**L**[3])]Cl (*E*-**3a**; middle trace), and [RuCl(cymene)(*Z*-**L**[3])]Cl (*Z*-**3a**; lower trace) in DMSO-d_6, immediately after dissolution; solvent (*) and ethanol signals (**) are marked with asterisks; for an enlarged view of the aromatic region (6.8–9.6 ppm), see Figure S11.

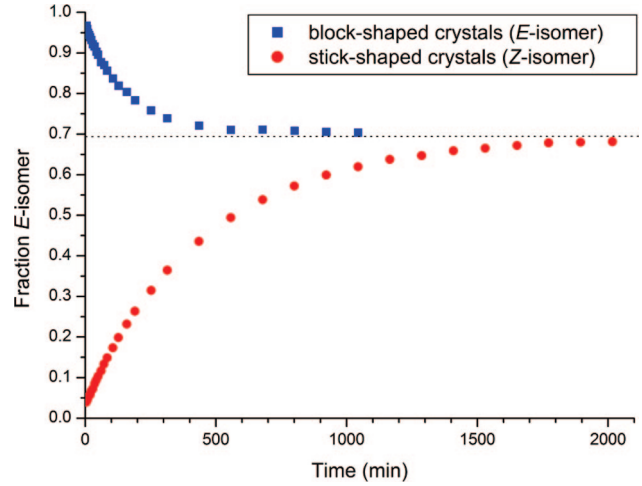

Figure 5. *E*/*Z* isomerization of *E*- and *Z*-**3a** in methanol-d_4.

Table 1. ^{1}H NMR Kinetic Studies on the *E*/*Z* Isomerization of **1–3** Starting from the Corresponding *Z*-Isomers ($E_0 \approx 0$) at 24 °C

solvent	cmpd	E_0[a]	E_∞[b]	K[c]	ΔG_{ZE}[d] (kJ/mol)	$t_{1/2}$[e] (min)	k_{ZE}[f] ($10\ s^{-1}$)	k_{EZ}[f] ($10^{-4}\ s^{-1}$)
DMSO-d_6	**1a**	0.018	0.424	0.736	0.76	92	0.458 ± 0.003	0.631 ± 0.006
	1b	0.010	0.339	0.513	1.65	142	0.213 ± 0.002	0.417 ± 0.005
	2a	0.096	0.381	0.616	1.20	16	1.0 ± 0.1	1.7 ± 0.2
	2b	0.007	0.289	0.407	2.23	335	0.0715 ± 0.0008	0.176 ± 0.003
	3a	0.002	0.267	0.364	2.50	865	0.0245 ± 0.0004	0.068 ± 0.002
	3b	0.077	0.183	0.224	3.71	34	0.14 ± 0.01	0.64 ± 0.06
methanol-d_4	**1a**	0.016	0.917	11.048	−5.95	66	8.8 ± 0.3	0.820 ± 0.009
	1b	0.071	0.884	7.621	−5.03	13	40 ± 2	4.9 ± 0.1
	2a	0.019	0.850	5.667	−4.30	170	1.85 ± 0.04	0.353 ± 0.004
	2b	0.070	0.815	4.405	−3.67	35	7.01 ± 0.07	1.61 ± 0.01
	3a	0.033	0.696	2.290	−2.05	313	0.410 ± 0.002	0.186 ± 0.001
	3b	0.140	0.627	1.681	−1.29	7	12.8 ± 0.3	7.7 ± 0.2

[a] E_0 represents the amount of the *E*-isomer at the beginning of the experiment, given as the fraction $E/(E + Z)$; the values were obtained by ^{1}H NMR integration of cymene methyl protons H^{28} and H^{29} for *E*- and *Z*-isomers. [b] E_∞ represents the amount of the *E*-isomer at equilibrium, given as the fraction $E/(E + Z)$; the values were obtained by ^{1}H NMR integration of cymene methyl protons H^{28} and H^{29} for *E*- and *Z*-isomers. [c] $K = E_\infty/Z_\infty$, with $Z_\infty = 1 - E_\infty$. [d] $\Delta G_{ZE} = -RT\ln K$. [e] The time necessary to reach $(E_0 + E_\infty)/2$, as determined experimentally. [f] Pseudo first-order rate constants for the *E*/*Z* isomerization process obtained by fitting first-order kinetics to experimental data; k_{ZE} refers to the partial reaction $Z \rightarrow E$ and k_{EZ} refers to $E \rightarrow Z$.

Table 2. ^{1}H NMR Kinetic Studies of *E*-**3a** at Different Concentrations at 24 °C

solvent	concn (mM)	E_0[a]	E_∞[b]	$t_{1/2}$[c] (min)	k_{ZE}[d] ($10^{-4}\ s^{-1}$)	k_{EZ}[e] ($10^{-4}\ s^{-1}$)
DMSO-d_6	5	0.882	0.266	11	5.36 ± 0.08	14.8 ± 0.2
	7.5	0.904	0.261	78	0.60 ± 0.02	1.62 ± 0.06
	10	0.930	0.253	265	0.27 ± 0.03	0.45 ± 0.03
	20	0.912	0.252	418	0.137 ± 0.001	0.410 ± 0.001
methanol-d_4	5	0.979	0.697	101	0.545 ± 0.008	0.227 ± 0.003
	7.5	0.971	0.694	119	0.488 ± 0.005	0.207 ± 0.002
	10	0.971	0.692	162	0.343 ± 0.003	0.152 ± 0.001
	15[f]	0.959	0.687	183	0.308 ± 0.001	0.140 ± 0.001

[a,b,c,d,e] See legend to Table. [f] 20 mM solutions are not accessible in methanol-d_4 due to reduced solubility compared to DMSO-d_6 as solvent.

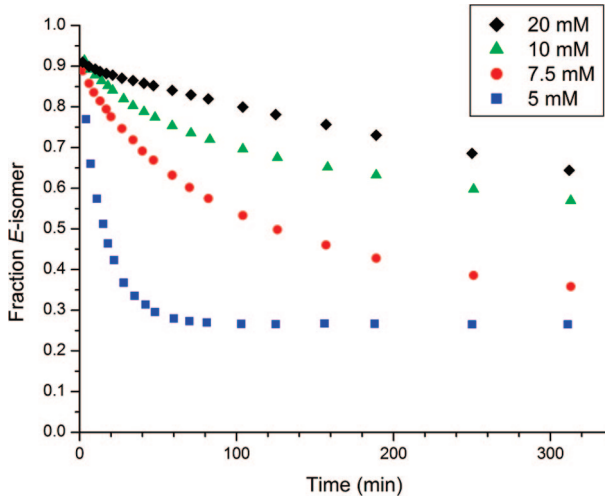

Figure 6. Concentration dependence of the *E*/*Z* isomerization of **3a** in DMSO-d_6.

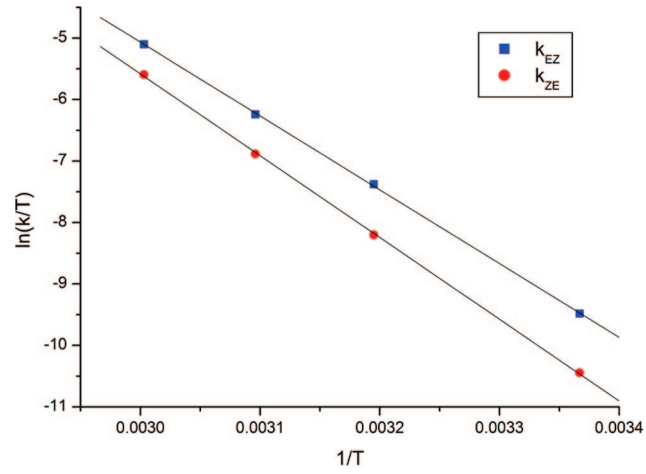

Figure 7. Eyring plot for the *E*/*Z* isomerization of **3a** at 24, 40, 50, and 60 °C.

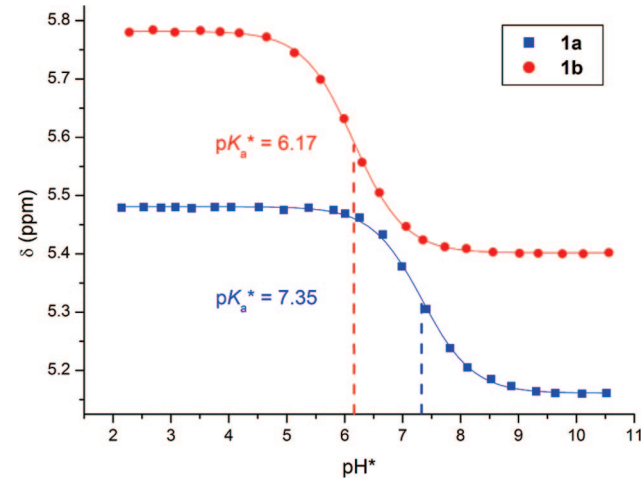

Figure 8. Dependence of the chemical shifts of cymene protons on pH* in the aqua complexes of *E*-**1a** and *E*-**1b**.

of 2.102(6), 2.082(6), 2.3786(18), and 1.694 Å (**4a**) and 2.091(3), 2.080(3), 2.3820(10), and 1.687 Å (**4b**).

***E*/*Z* Isomerization Behavior of 1–3.** The reaction half-lives $t_{1/2}$ depend significantly on both the solvent and the metal and vary between 7 and 865 min. In DMSO-d_6, the *E*/*Z* equilibrium for ruthenium complexes **1a** and **2a** is reached faster than for the osmium complexes **1b** and **2b**, whereas this tendency is reversed in methanol-d_4. For the osmium complex **3b**, the equilibrium is reached faster than for the ruthenium complex **3a** in both solvents (Tables 1 and S4). At equilibrium, the *Z*-isomers predominate in DMSO-d_6 and the *E*-isomers predominate in methanol-d_4. Regardless of solvent and reaction half-life, equilibrium mixtures of the osmium complexes always contain a lower fraction of the *E*-isomer than those of their ruthenium congeners. A nitro substituent in position 9 instead of H or Br affects the *E*/*Z* equilibrium in such a way that the amount of the *E*-isomer is significantly lower in both solvents and with both metals.

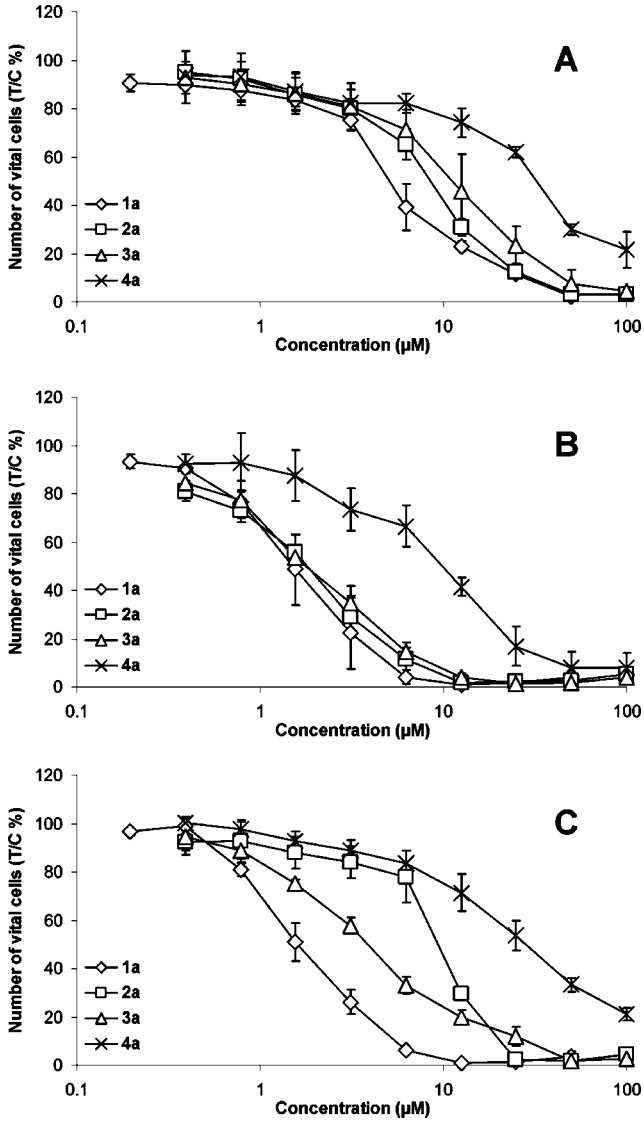

Figure 9. Concentration−effect curves of the ruthenium complexes **1a**–**4a** in (A) A549, (B) CH1, and (C) SW480 cells, obtained by the MTT assay. Values are means ± standard deviations from at least three independent experiments.

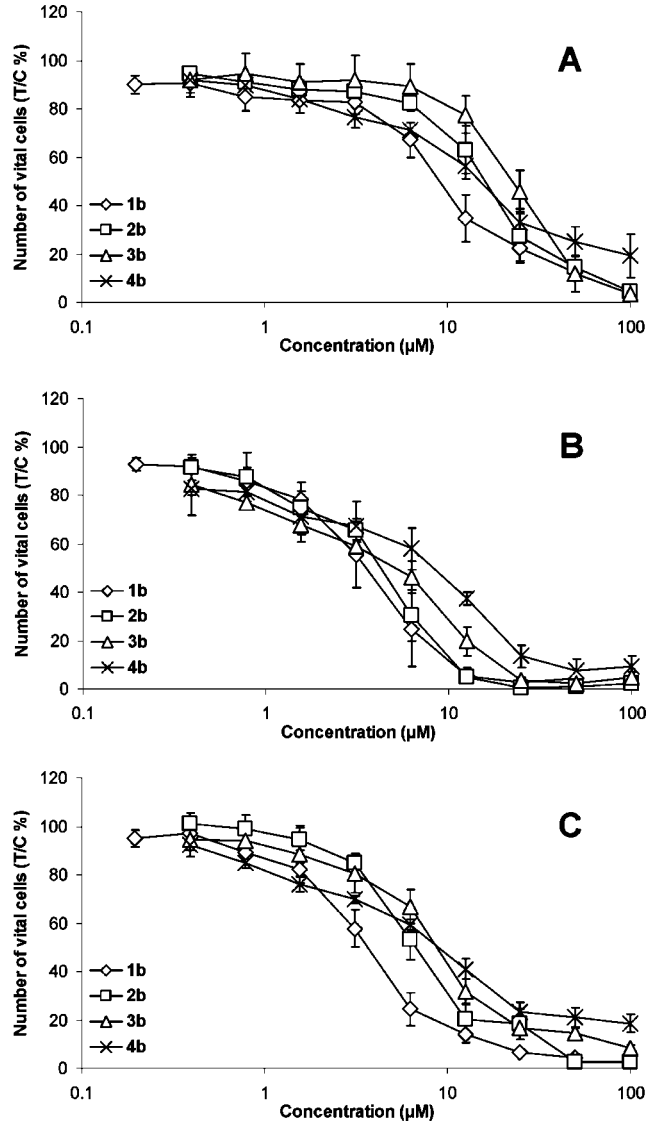

Figure 10. Concentration−effect curves of the osmium complexes **1b**–**4b** in (A) A549, (B) CH1, and (C) SW480 cells, obtained by the MTT assay. Values are means ± standard deviations from at least three independent experiments.

Longer reaction times were necessary to reach equilibrium when starting from more concentrated solutions of **3a** in both DMSO-d_6 and methanol-d_4. The concentration dependence was more pronounced in DMSO-d_6: 5 mM solutions showed $t_{1/2}$ = 11 min compared to $t_{1/2}$ = 265 min of 10 mM solutions, which corresponds to an about 24-fold increase in time necessary to reach half the equilibrium concentration of the *E*-isomer (Figure 6). In methanol-d_4, $t_{1/2}$ = 101 min for the 5 mM solution increased only by a factor of about 1.6 to $t_{1/2}$ = 162 min for the 10 mM solution (Tables 2 and S5). UV–vis spectra of *E*- and *Z*-**3a** show practically identical absorbance features, as is also observed for *E*- and *Z*-isomers of comparable rhenium α-picolylcarboxaldimine complexes.[38] However, we cannot exclude that equilibration is too fast to detect possible differences at the low concentrations used (0.02 mM).

According to the Gibbs–Helmholtz equation, the determined $\Delta H^{\ddagger}$ and $\Delta S^{\ddagger}$ values for the *E*/*Z* isomerization of **3a** result in $\Delta G^{\ddagger}_{ZE}$ = 84.5 ± 1.4 kJ/mol and $\Delta G^{\ddagger}_{EZ}$ = 82.1 ± 1.5 kJ/mol at 24 °C. Thus, the Gibbs free enthalpy ΔG_{ZE} of 2.50 kJ/mol, as determined from the corresponding equilibrium constant *K* of **3a** (Table 1), is in good agreement with these values.

Table 3. Cytotoxicity of Compounds **1**−**4**

	IC_{50}[a] (μM)		
cmpd	A549	CH1	SW480
1a	5.2 ± 0.9	1.6 ± 0.5	1.6 ± 0.3
1b	9.2 ± 1.6	3.7 ± 1.0	3.7 ± 0.6
2a	8.5 ± 0.7	1.9 ± 0.4	1.2 ± 0.5
2b	16 ± 3	4.5 ± 1.0	6.7 ± 1.0
3a	12 ± 4	1.8 ± 0.2	3.9 ± 0.3
3b	23 ± 4	5.5 ± 1.0	8.7 ± 1.0
4a	32 ± 1	9.7 ± 1.6	28 ± 5
4b	15 ± 2	7.9 ± 1.3	9.0 ± 1.0

[a] 50% inhibitory concentrations in A549, CH1, and SW480 cells after exposure for 96 h in the MTT assay. Values are means ± standard deviations, obtained from at least three independent experiments.

Rotation around the predominantly double bond $C^6{=}N^{13}$ has to occur to effect *E*/*Z* isomerization. For imines[39] and amidines,[40] the underlying mechanisms and their contributions to the overall isomerization rate have been investigated. To the best of our knowledge, coordinated amidines have not yet been studied in this regard. We assume that the complex dependence pattern we observed is due to an interplay of several factors.

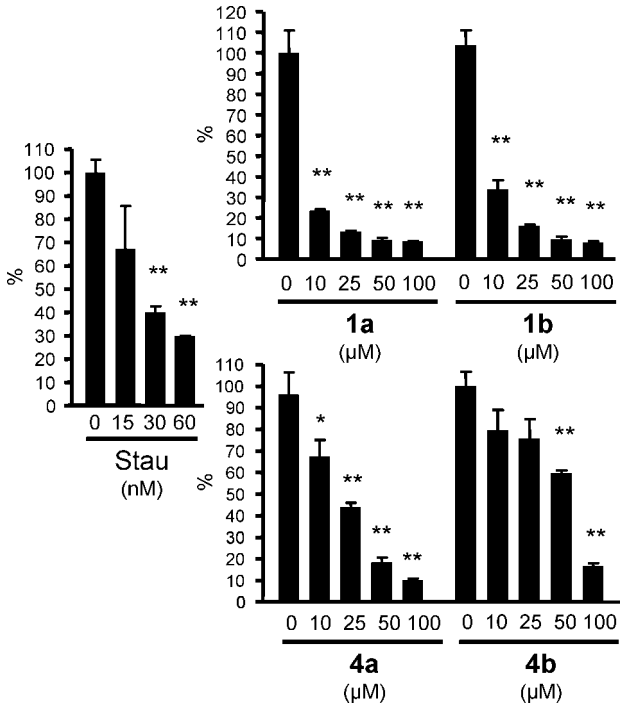

Figure 11. Impact of **1a**, **1b**, **4a**, and **4b** on DNA synthesis, as determined by ^{3}H-thymidine incorporation assays after 24 h with the indicated drug concentrations. ** (*) Significantly [$p < 0.01$ ($p < 0.05$)] different from untreated control by one-way ANOVA and Dunnet test.

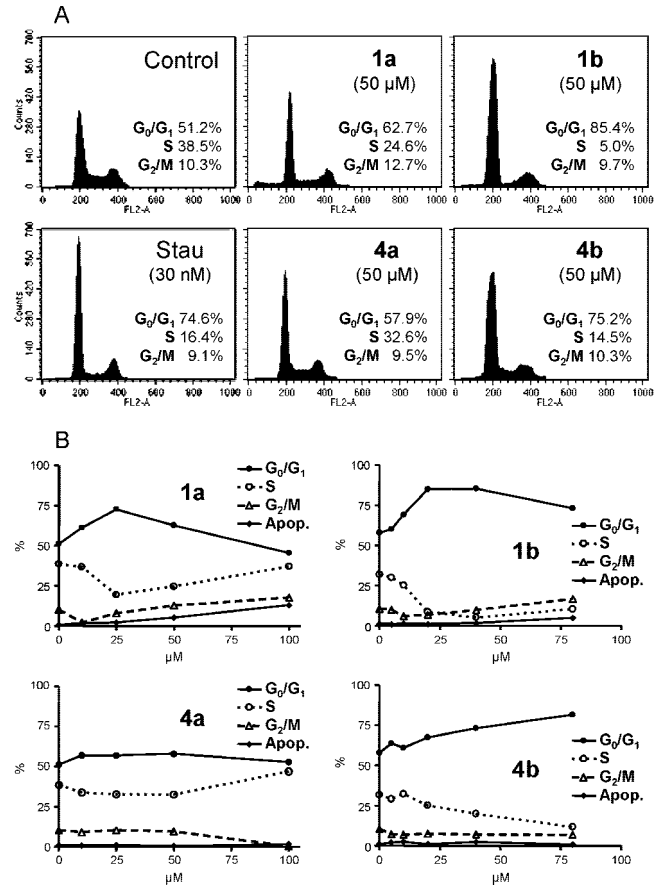

Figure 12. Impact of **1a**, **1b**, **4a**, and **4b** on cell cycle distribution. (A) Fluorescence intensity as a measure for the DNA content of PI-stained A549 cells after a 24 h treatment with the indicated drug concentrations, as analyzed by flow cytometry. (B) Percentages of PI-stained A549 cells in G_0/G_1, *S*, and G_2/M phase after 24 h treatment with the indicated drug concentrations, as calculated by Cell Quest software.

Because the $C^6{=}N^{13}$ bond was found to be longer than typical C=N double bonds in the solid state and in the metal-free paullone-based ligands, $\mathbf{L^1}$, $\mathbf{L^2}$, and $\mathbf{L^3}$, another tautomer with endocyclic double bond was observed, it seems conceivable that a further reduction in bond order is achieved by tautomerization. This process can be proton-catalyzed and would thus be dependent on the basicity of the nitrogen atom to be protonated (N^{13}) and on the proton concentration. The former might be altered by binding to the metal, as we actually observed. The paullone ligands presented herein possess also other nitrogen atoms as possible proton acceptors, and it is known[41] that electron-withdrawing substituents in position 9 increase the basicity of N^{12}. This could explain the impact of the ligand substitution in this position even if the metal, the concentration, and the solvent are not varied. Possibly, the basicity of the paullone ligands also leads to the observed lower isomerization rate if the concentration is increased. The higher proportion of *E*-isomers at equilibrium in methanol-d_4 might be explained by a better stabilization of the $N{-}H^5{\cdots}Cl^1$ hydrogen bonds in this protic solvent as compared to the aprotic DMSO-d_6.

Solution Structures of Complexes 1–3. $^1H{-}^1H$ ROESY NMR experiments performed immediately after sample dissolution provide direct evidence for the difference in 3D structure of *E*- and *Z*-isomers in solution. The *Z*-isomer of **3a** shows crosspeaks between the α-picolylamine methylene group H^{14} and the amidine nitrogen proton H^5, which are, as expected, not observed in the spectrum of the *E*-isomer (Figures S12 and S14). With this experiment, also the proton resonances of each of the two methylene groups ($H^7{}_a$, $H^7{}_b$, and $H^{14}{}_a$, $H^{14}{}_b$) can be distinguished.

From the crystal structures, it is evident that in the *Z*-isomeric complexes, the azepine methylene group points toward the cymene ligand, whereas it points away in the complexes with *E*-configuration (*vide supra*). Because NOE crosspeaks from $H^7{}_a$ and $H^7{}_b$ toward cymene protons are significantly stronger for *Z*-**3a** than for *E*-**3a**, it can be concluded that this ligand twist is likely retained in solution.

With the exception of *Z*-**3a**, only the cymene ligand orientation with the isopropyl group above C^{14} of the paullone chelate ring is observed in all studied X-ray structures, (*vide supra*). From NOE crosspeaks between paullone and cymene protons, it is evident that, additionally, also another cymene orientation exists in solution, as indicated in Chart 2. Taking into account the relative NOE intensities, the isopropyl group in orientation A is preserved but is slightly rotated away from the paullone scaffold when compared to the structure observed in the solid state, lying approximately above C^{14a} instead of C^{14}. Orientation B is obtained from the solid state structure by 180° rotation of the cymene ligand about the ruthenium-centroid vector so that the methyl group resides above C^{14} instead of the isopropyl group.

For *E*- and *Z*-**3a**, crosspeaks between H^{18} and all four aromatic cymene protons (Figures S12 and S13) and between $H^{14}{}_a$ and the cymene isopropyl and methyl groups are observed (Figures S13 and S15). The corresponding NOE intensities are similar for the *E*-isomer, which indicates an equal population of cymene orientations A and B. For the *Z*-isomer, however, the NOE H^{18}/H^{22} is stronger than H^{18}/H^{25}, and $H^7{}_b/H^{25}$ is stronger than $H^7{}_b/H^{22}$. Hence, for this isomer, cymene orientation A is preferred in solution over orientation B (Table S3). A similar situation has been described in the literature,[34] where the cymene orientation with the isopropyl group above the

chelate ring was observed in the solid state and in solution a second orientation differing from the first by 180° rotation of the *p*-cymene ligand could be deduced from NOE contacts. ^{1}H and ^{13}C NMR spectra of **1a**, **1b**, **2a**, **2b**, and **3b** are similar to those of **3a** (Tables S6−S13) and, as a consequence, no different structures can be expected in solution.

The complexes **1**–**3** display two signal sets corresponding to the *E*- and *Z*-isomers. In addition to the *R*/*S*-configuration at the metal ion, these complexes possess two other sources of chirality. One is the δ/λ chirality of the chelate ring, and the other is the planar chirality of the paullone ligand, which can be characterized by the sign of the torsion angle $\Theta_{N1\text{-}C5\text{-}C6\text{-}C7}$. The fact that only one signal set for each *E*- and *Z*-isomer is observed demonstrates that, in agreement with their structures in the solid state, only the enantiomeric pairs $S_{Os}\delta\Theta_{+}/R_{Os}\lambda\Theta_{-}$ exist in solution.[42]

Solution Structures of Complexes 4a and 4b. Because their Schiff base double bond is located in the chelate ring, *E*/*Z*-isomerization is impossible in **4a** and **4b**. The structure of these complexes in solution was derived from the ^{1}H−^{1}H ROESY spectrum of **4a** (Figures S16 and S17). As the NOE H^{14}/H^8 is more intense than H^{14}/H^{10} (Figure S17), the chelating moiety is rotated out of the plane of the paullone indole ring with a torsion angle $|\Theta_{C14\text{-}N13\text{-}C9\text{-}C10}|$ of over 90° so that H^{14} is closer to H^8 than to H^{10}. This finding is in agreement with the solid state structures of **4a** and **4b**, where the corresponding torsion angle ($\Theta_{C13\text{-}N3\text{-}C1\text{-}C2}$ in the atom numbering used for X-ray structures) was found to be −124.9(7) and 125.8(4)°, respectively. The orientation of the cymene ligand can be deduced from the intensity of (i) crosspeaks between H^8, H^{10} and aromatic cymene protons decreasing in the order H^{25} > H^{24} > H^{23} ≈ H^{22} and (ii) crosspeaks between H^{18} and aromatic cymene protons decreasing in the order H^{23} > H^{22} > H^{24} > H^{25}. Thus, cymene ligand orientation B is preferred over A in solution (Table S3). ^{1}H and ^{13}C NMR spectra of **4b** are similar to those of **4a** (Tables S12 and S13), and, as a consequence, no different structures can be expected in solution. Only one signal set is observed for **4a** and **4b** because they exist as *R*/*S*-enantiomeric pairs in solution.

Cytotoxicity, ^{3}H-Thymidine Incorporation Assay and Cell Cycle Analysis. A comparison with the activity patterns of the metal-free paullone derivatives was not possible because of their aqueous insolubility. Consistent structure–activity relationships can be deduced for the central metal in the complexes with the chelating moiety derived from the lactam unit. The osmium complexes **1b**–**3b** are slightly (about two times) less active in all three cell lines than their ruthenium analogs **1a**–**3a**, but their IC_{50} values are still mostly in the 10^{-6} M range. This contrasts with the osmium arene compounds investigated by Sadler and co-workers, which seemed to be devoid of activity in concentrations up to 100 μM, as opposed to their ruthenium congeners,[35] with few notable exceptions.[10,43] Inertness to formation of biologically inactive hydroxo-bridged dinuclear species $[(\eta^6\text{-}p\text{-cymene})M(\mu\text{-}OH)_3M(\eta^6\text{-}p\text{-cymene})]^+$ (M = Os) has been a tentative explanation for these exceptions. Consistent with this notion, no formation of such dimeric species has been observed with any of the biologically active compounds **1**–**4** (M = Ru, Os).

Although variation of the ligand has a more pronounced impact on antiproliferative activity, structure–activity relationships are less clear-cut in this respect. The complexes containing the ligand $\mathbf{L^1}$, which is unsubstituted in position 9 (**1a**, **1b**), tend to be the most active within their respective series, in line with previous results obtained with closely related compounds,[28] but differences to the complexes containing the bromo- or nitro-substituted ligands $\mathbf{L^2}$ or $\mathbf{L^3}$ become conspicuous only within the ruthenium series in SW480 cells. On the other hand, the position of the chelating moiety as in compound **4a** brings about a marked decrease of activity in the case of ruthenium but not osmium, inverting the metal-dependent effects mentioned above. This latter finding conflicts with the assumption that differences in susceptibility to hydrolysis may explain differences in antiproliferative activity, because the ruthenium complexes hydrolyze to a greater extent than their osmium congeners irrespective of the position of the chelating moiety.

A comparison with related ruthenium compounds, each containing a second ligand molecule $\mathbf{L^1}$ or $\mathbf{L^2}$ and one dimethyl sulfoxide and chloro ligand,[28] reveals that the change to an organometallic moiety not only results in increased solubility, but also in markedly increased antiproliferative activity in all three cell lines.

Because only minor binding to 5′-GMP was observed, covalent binding to DNA does not appear to be the crucial mode of action. It seems more likely that intercalation or interference with another intracellular target (e.g., CDKs for **4a** and **4b**) leads to the observed cytotoxicity.

All experiments addressing antiproliferative activity, DNA synthesis, and cell cycle distribution come to the same result that **1a** and **1b** are more potent agents than **4a** and **4b**. This is particularly remarkable, as the position of the chelating moiety at the lactam unit in compounds **1a** and **1b** should, in contrast to its position in compounds **4a** and **4b**, be incompatible with binding to the ATP binding site of CDKs.[21] Further studies are required to clarify whether direct effects on CDKs are involved in the mechanism of action of these compounds or whether molecular effects other than CDK inhibition account for their antiproliferative effects.

Conclusion

The first organometallic arene complexes of paullone-based ligands have been synthesized and characterized by spectroscopic methods and X-ray diffraction. Compared to paullone coordination compounds, they are accessible in higher yield. The cationic complexes hydrolyze slowly in solutions with high water content. Those complexes featuring a coordinated amidine unit (**1**−**3**) were found to be subject to *E*/*Z* isomerization in solution. With the exception of **3a**, the ruthenium complexes reached equilibrium faster than the osmium complexes and led to a higher amount of the *Z*-isomer at equilibrium in DMSO-d_6, whereas the opposite situation was encountered in methanol-d_4. More concentrated solutions of the complexes in DMSO-d_6 reacted more slowly than less concentrated solutions. This concentration dependence was found to be significantly less pronounced in methanol-d_4. Remarkably, the paullone complexes with a derivatized lactam unit showed higher antiproliferative activity than the first paullone complexes with unmodified lactam unit. For all complexes, IC_{50} values lie in the low micromolar range, reasonable for potential antitumor drugs. The observed reduction in DNA synthesis activity and G_0/G_1 arrest at low micromolar concentrations are pronounced for **1a** and **1b** and are in line with their high cytotoxicity. Whether inhibition of CDKs indeed accounts for these effects will be elucidated by suitable techniques.

Experimental Section

Elemental analyses were carried out by the Microanalytical Service at the Institute of Physical Chemistry of the University of Vienna. Thermogravimetric and differential thermal analyses were

performed on a Mettler Toledo TGA/SDTA851e instrument. Ethanol and residual water were firmly incorporated into the crystal lattice of the complexes and could not be completely removed on drying in vacuo. The content of ethanol in the samples was determined by integration of ^{1}H NMR spectra and used for the calculation of the compositions of the prepared compounds. The water content was determined by fitting to elemental analyses and verified by thermogravimetric measurements. Infrared spectra were recorded on a Perkin-Elmer FT-IR 2000 spectrometer in KBr (4000–400 cm^{-1}). UV–vis spectra were measured on a Perkin-Elmer Lambda 650 UV–vis spectrophotometer using samples dissolved in methanol or DMSO−water. Electrospray ionization mass spectrometry was carried out with a Bruker Esquire 3000 instrument with solutions of the compounds in methanol. Expected and experimental isotope distributions were compared and *m*/*z* values were quoted for the species with highest natural abundance. Cyclic voltammograms were measured in a three-electrode cell using a 0.2 mm diameter glassy carbon working electrode, a platinum auxiliary electrode, and a $Ag|Ag^+$ reference electrode containing 0.1 M $AgNO_3$. Measurements were performed at room temperature using an EG & PARC 273A potentiostat/galvanostat. Deaeration of solutions was accomplished by passing a stream of argon through the solution for 5 min prior to the measurements and then maintaining a blanket atmosphere of argon over the solutions during the measurements. The potentials were measured in 0.15 M [*n*-Bu_4N][BF_4]/DMF, using [Fe(η^5-C_5H_5)$_2$] ($E_{1/2}$ = +0.72 V vs NHE)[44] as internal standard and were quoted relative to NHE.

NMR Spectroscopy. ^{1}H, ^{31}P, ^{13}C, and two-dimensional ^{1}H−^{1}H COSY, ^{1}H−^{1}H TOCSY, ^{1}H−^{1}H ROESY, ^{1}H−^{13}C HMQC, and ^{1}H−^{13}C HMBC NMR spectra were recorded with Bruker Avance DPX™ 400 (^{1}H 400.13, ^{31}P 161.98, ^{13}C 100.63 MHz) or Bruker Avance III 500 (^{1}H 500.10, ^{31}P 202.44 MHz) spectrometers in DMSO-d_6, methanol-d_4, or D_2O/DMSO-d_6 = 90:10 at 24 °C using standard pulse programs. Two-dimensional spectra were measured in a gradient-enhanced mode. ^{1}H and ^{13}C chemical shifts are referenced relative to the solvent signals. ^{1}H NMR titration studies were performed in the range pH* 2−11 (pH* obtained by pH meter reading without correction for effects of D on glassy electrode) in steps of about pH* 0.3–0.4 with a pH meter Eutech Ecoscan pH6 equipped with an Orion 9826BN pH electrode. The obtained chemical shifts for the aqua complexes were plotted versus pH* and pK_a* values (pK_a values for solutions in D_2O) were determined by fitting to the Henderson–Hasselbalch equation, with the assumption that the observed chemical shifts are weighted averages according to the populations of the aqua and hydroxo species. For comparison with other literature data, these can be converted into pK_a values by the equation pK_a = 0.929 pK_a* + 0.42, suggested by Krezel and Bal.[45]

Crystallographic Structure Determination. X-ray diffraction measurements were performed on a Bruker X8 APEXII CCD diffractometer. Single crystals were positioned at 40 mm from the detector, and 1032, 2623, 1511, 2960, 1301, 2682, 1595, and 1578 frames were measured, each for 80, 30, 10, 3, 10, 20, 20, and 20 s over 1° scan width for **L^3**, *Z*-**1b**, *Z*-**2b**, *E*-**3a**, *Z*-**3a**, *E*-**3b**, **4a**, and **4b**, correspondingly. The data were processed using SAINT software.[46] Crystal data, data collection parameters, and structure refinement details are given in Table S1. The structures were solved by direct methods and refined by full-matrix least-squares techniques. Non-H atoms were refined with anisotropic displacement parameters. H atoms were inserted in calculated positions and refined with a riding model. The following computer programs were used: structure solution, SHELXS-97;[47] refinement, SHELXL-97;[48] molecular diagrams, ORTEP;[49] computer, Pentium IV; scattering factors.[50]

Cell Lines and Culture Conditions. A549 cells (nonsmall cell lung carcinoma) and SW480 cells (adenocarcinoma of the colon) were obtained from the American type Culture Collection (ATCC) and kindly provided by Brigitte Marian, Institute of Cancer Research, Medical University of Vienna, Austria. CH1 cells originate from an ascites sample of a patient with a papillary cystadenocarcinoma of the ovary and were kindly provided by Lloyd R. Kelland, CRC Centre for Cancer Therapeutics, Institute of Cancer Research, Sutton, U.K. Cells were grown in 75 cm^2 culture flasks (Iwaki) as adherent monolayer cultures in complete culture medium, that is, Minimal Essential Medium (MEM) supplemented with 1 mM sodium pyruvate, 4 mM L-glutamine, 1% nonessential amino acids (100×; all purchased from Sigma-Aldrich), and 10% heat-inactivated fetal bovine serum (purchased from Invitrogen). Cultures were maintained at 37 °C in a humidified atmosphere containing 5% CO_2.

Cytotoxicity Tests in Cancer Cell Lines. Cytotoxicity was determined by means of a colorimetric microculture assay (MTT assay, MTT = 3-(4,5-dimethyl-2-thiazolyl)-2,5-diphenyl-2*H*-tetrazolium bromide, purchased from Fluka). For this purpose, A549, CH1, and SW480 cells were harvested from culture flasks by trypsinization and seeded into 96-well microculture plates (Iwaki). The following cell densities were chosen to ensure exponential growth throughout drug exposure: 4 × 10^3 cells/well (A549), 1.5 × 10^3 cells/well (CH1), and 2.5 × 10^3 cells/well (SW480). After a 24 h preincubation, cells were exposed to solutions of the test compounds in 200 μL/well complete culture medium for 96 h. At the end of exposure, drug solutions were replaced by 100 μL/well RPMI1640 culture medium (supplemented with 10% heat-inactivated fetal bovine serum) plus 20 μL/well MTT solution in phosphate-buffered saline (5 mg/ml PBS). After incubation for 4 h, the medium/MTT mixtures were removed, and the formazan crystals formed by the mitochondrial dehydrogenase activity of vital cells were dissolved in 150 μL of DMSO per well. Optical densities at 550 nm were measured with a microplate reader (Tecan Spectra Classic), using a reference wavelength of 690 nm to correct for unspecific absorption. The quantity of vital cells was expressed in terms of *T*/*C* values by comparison to untreated control microcultures, and IC_{50} values were calculated from concentration−effect curves by interpolation. Evaluation is based on means from at least three independent experiments, each comprising six microcultures per concentration level.

^{3}H-Thymidine Incorporation Assay. A549 cells (5 × 10^3 cells/well) were seeded in a 96-well plate and treated 24 h later with the test substances for another 24 h. Medium was replaced by a 2 nM ^{3}H-thymidine solution (diluted in complete culture medium; radioactivity 25 Ci/mM). After 1 h incubation at 37 °C, cells were washed three times with PBS. Cell lysates were prepared and the radioactivity determined as described previously.[51]

Cell Cycle Analysis. A549 cells (5 × 10^5 cells/well) were seeded into six-well plates and allowed to recover for 24 h. After recovery, cells were exposed to the test compounds for 24 h. Control and drug-treated cells were collected, washed with PBS, fixed in 70% ice-cold ethanol, and stored at −20 °C. To determine cell cycle distribution, cells were transferred into PBS, incubated with RNase A (10 μg/mL) for 30 min at 37 °C, followed by a 30 min treatment with 5 μg/mL propidium iodide. Fluorescence levels were analyzed by flow cytometry using a FACS (fluorescence-assisted cell sorting) Calibur instrument (Becton Dickinson, Palo Alto, CA). The resulting DNA histograms were quantified using Cell Quest Pro software (Becton Dickinson and Company, New York, U.S.A.).

Starting Materials. 9-Nitro-7,12-dihydroindolo[3,2-*d*][1]benzazepin-6(5*H*)-thione,[21] 9-amino-7,12-dihydroindolo[3,2-*d*][1]benzazepin-6(5*H*)-one,[52] 6-(α-picolylamino)-7,12-dihydroindolo[3,2-*d*][1]benzazepine (**L^1**),[28] 9-bromo-6-(α-picolylamino)-7,12-dihydroindolo[3,2-*d*][1]benzazepine (**L^2**),[28] [$Ru^{II}Cl(\mu$-Cl)(η^6-*p*-cymene)]$_2$,[53] and [$Os^{II}Cl(\eta^6$-*p*-cymene)]$_2$[54] have been prepared according to published protocols. Tetrahydrofuran (THF) and ethanol were dried using standard procedures. α-Picolylamine and 2-pyridinecarbaldehyde were purchased from Acros and Merck, respectively, and used without further purification. ^{1}H and ^{13}C NMR, conductometric, IR, and UV–vis spectral data and elemental analyses of all compounds are given in the Supporting Information.

Synthesis of Ligands. 9-Nitro-6-(α-picolylamino)-7,12-dihydroindolo[3,2-*d*][1]benzazepine (L^3). To 9-nitro-7,12-dihydroindolo[3,2-*d*][1]benzazepin-6(5*H*)-thione (2.00 g, 6.4 mmol) in dry THF (100 mL), α-picolylamine (1.4 mL, 12.8 mmol) was added and the solution was refluxed for 24 h. After cooling to room

temperature, the mixture was filtered and the filtrate was evaporated to dryness. The obtained solid was extracted with acetone (150 mL), the extract was concentrated to about half the volume and left to stand at –20 °C for 1 week. The yellow precipitate was filtered off, washed with diethyl ether, and dried in vacuo. Further fractions were obtained by concentrating the acetone solution to about half the volume and crystallization at −20 °C. Yield: 1.61 g, 63%. Anal. ($C_{22}H_{17}N_5O_2$) C, H, N. Mp 220 °C (dec). MS (ESI+) *m/z* 406 [$\mathbf{L^3}$ + Na]$^+$, 384 [$\mathbf{L^3}$ + H]$^+$; (ESI−) *m/z* 418 [$\mathbf{L^3}$ + Cl]$^-$, 382 [$\mathbf{L^3}$ − H]$^-$. Single crystals suitable for X-ray diffraction study were grown by slow diffusion of pentane into a solution of $\mathbf{L^3}$ in acetone at 4 °C.

9-(Pyridin-2-ylmethylidene)amino-7,12-dihydroindolo[3,2-*d*][1]benzazepin-6(5*H*)-one ($\mathbf{L^4}$). To a boiling solution of 2-pyridinecarbaldehyde (1.0 mL, 11.4 mmol) in methanol (20 mL), a solution of 9-amino-7,12-dihydroindolo[3,2-*d*][1]benzazepin-6(5*H*)-one (1.4 g, 5.3 mmol) in methanol (200 mL) was added dropwise over 2 h. The mixture was refluxed for 30 min, allowed to cool to room temperature, and left to stand at 4 °C for 2 h. The yellow solid was filtered off, washed with methanol, and dried in vacuo at 80 °C. Yield: 1.45 g, 78%. Anal. ($C_{22}H_{16}N_4O$) C, H, N. Mp 300 °C (dec). MS (ESI+) *m/z* 727 [2 $\mathbf{L^4}$ + Na]$^+$, 375 [$\mathbf{L^4}$ + Na]$^+$, 353 [$\mathbf{L^4}$ + H]$^+$; (ESI−) *m/z* 387 [$\mathbf{L^4}$ + Cl]$^-$, 351 [$\mathbf{L^4}$ − H]$^-$.

Synthesis of Complexes. Synthesis of Ruthenium(II) and Osmium(II) Arene Complexes of $\mathbf{L^1}$−$\mathbf{L^3}$. General Procedure A. A mixture of 6-(α-picolylamino)-7,12-dihydroindolo-[3,2-*d*][1]benzazepine ($\mathbf{L^1}$) or its 9-bromo ($\mathbf{L^2}$) or 9-nitro ($\mathbf{L^3}$) derivative ($\mathbf{L^1}$, 0.34 g; $\mathbf{L^2}$, 0.42 g; $\mathbf{L^3}$, 0.38 g, 1.0 mmol) and [M^{II}Cl(μ-Cl)(η^6-*p*-cymene)]$_2$ (M = Ru, Os; Ru, 0.31 g; Os, 0.39 g, 0.5 mmol) was refluxed in dry ethanol (40 mL) for 1 h and allowed to cool to room temperature. Hexane was added under stirring until a slight turbidity was observed. The mixture was left to stand at 4 °C for 2 h and filtered. Then the filtrate was allowed to stand at 4 °C for 2 weeks. ($\mathbf{L^1}$: After 1 week, 10 mL of diethyl ether was added to reduce phase separation.) The yellow crystals were filtered off, washed with diethyl ether, and dried in vacuo.

Synthesis of Ruthenium(II) and Osmium(II) Arene Complexes of $\mathbf{L^4}$. General Procedure B. 9-(Pyridin-2-ylmethylidene)amino-7,12-dihydroindolo[3,2-*d*][1]benzazepin-6(5*H*)-one ($\mathbf{L^4}$; 0.35 g, 1.0 mmol) and [M^{II}Cl(μ-Cl)(η^6-*p*-cymene)]$_2$ (M = Ru, Os; Ru, 0.31 g; Os, 0.39 g, 0.5 mmol) were stirred in dry ethanol (50 mL) for 45 min at room temperature. Hexane was added under stirring until a slight turbidity was observed. The mixture was left to stand at 4 °C for 2 h and filtered. Then the filtrate was allowed to stand at 4 °C for 2 weeks. The red crystals were filtered off, washed with diethyl ether, and dried in vacuo.

(η^6-*p*-Cymene){6-[(α-picolyl-κ*N*)imino-κ*N*]-7,12-dihydroindolo[3,2-*d*][1]benzazepine}chlororuthenium(II) Chloride, [RuCl(cymene)$\mathbf{L^1}$]Cl (1a). General Procedure A. Yield: 0.29 g, 42%. Anal. ($C_{32}H_{32}Cl_2N_4Ru$) C, H, Cl, N. Mp 220 °C (dec). MS (ESI+) *m/z* 609 [RuCl(cymene)$\mathbf{L^1}$]$^+$, 573 [RuCl(cymene)$\mathbf{L^1}$ − HCl]$^+$; (ESI−) *m/z* 643 [RuCl(cymene)$\mathbf{L^1}$ − H + Cl]$^-$, 607 [RuCl(cymene)$\mathbf{L^1}$ − 2H]$^-$.

(η^6-*p*-Cymene){6-[(α-picolyl-κ*N*)imino-κ*N*]-7,12-dihydroindolo[3,2-*d*][1]benzazepine}chloroosmium(II) Chloride, [OsCl(cymene)$\mathbf{L^1}$]Cl (1b). General Procedure A. Yield: 0.34 g, 44%. Anal. ($C_{32}H_{32}Cl_2N_4Os$) C, H, N. Mp 240 °C (dec). MS (ESI+) *m/z* 699 [OsCl(cymene)$\mathbf{L^1}$]$^+$, 663 [OsCl(cymene)$\mathbf{L^1}$ − HCl]$^+$; (ESI−) *m/z* 733 [OsCl(cymene)$\mathbf{L^1}$ − H + Cl]$^-$. X-ray diffraction-quality single crystals of **1b** could be selected directly from the reaction vessel.

(η^6-*p*-Cymene){9-bromo-6-[(α-picolyl-κ*N*)imino-κ*N*]-7,12-dihydroindolo[3,2-*d*][1]benzazepine}chlororuthenium(II) Chloride, [RuCl(cymene)$\mathbf{L^2}$]Cl (2a). General Procedure A. Yield: 0.48 g, 60%. Anal. ($C_{32}H_{31}BrCl_2N_4Ru$) C, H, Br, Cl, N. Mp 200 °C (dec). MS (ESI+) *m/z* 689 [RuCl(cymene)$\mathbf{L^2}$]$^+$, 653 [RuCl(cymene)$\mathbf{L^2}$ − HCl]$^+$; (ESI−) *m/z* 723 [RuCl(cymene)$\mathbf{L^2}$ − H + Cl]$^-$, 687 [RuCl(cymene)$\mathbf{L^2}$ − 2H]$^-$, 651 [RuCl(cymene)$\mathbf{L^2}$ − HCl − 2H]$^-$.

(η^6-*p*-Cymene){9-bromo-6-[(α-picolyl-κ*N*)imino-κ*N*]-7,12-dihydroindolo[3,2-*d*][1]benzazepine}chloroosmium(II) Chloride, [OsCl(cymene)$\mathbf{L^2}$]Cl (2b). General Procedure A. Yield: 0.56 g, 65%. Anal. ($C_{32}H_{31}BrCl_2N_4Os$) C, H, N. Mp 240 °C (dec). MS (ESI+) *m/z* 777 [OsCl(cymene)$\mathbf{L^2}$]$^+$, 741 [OsCl(cymene)$\mathbf{L^2}$ − HCl]$^+$; (ESI−) *m/z* 811 [OsCl(cymene)$\mathbf{L^2}$ − H + Cl]$^-$, 775 [OsCl(cymene)$\mathbf{L^2}$ − 2H]$^-$, 739 [OsCl(cymene)$\mathbf{L^2}$ − HCl − 2H]$^-$. Single crystals of **2b** suitable for X-ray diffraction study could be selected directly from the reaction vessel.

(η^6-*p*-Cymene){9-nitro-6-[(α-picolyl-κ*N*)imino-κ*N*]-7,12-dihydroindolo[3,2-*d*][1]benzazepine}chlororuthenium(II) Chloride, [RuCl(cymene)$\mathbf{L^3}$]Cl (3a). General Procedure A. Yield: 0.53 g, 70%. Anal. ($C_{32}H_{31}Cl_2N_5ORu$) C, H, Cl, N. Mp, *Z*-isomer, 220 °C (dec), *E*-isomer, 220 °C (dec). MS (ESI+) *m/z* 654 [RuCl(cymene)$\mathbf{L^3}$]$^+$, 618 [RuCl(cymene)$\mathbf{L^3}$ − HCl]$^+$; (ESI−) *m/z* 688 [RuCl(cymene)$\mathbf{L^3}$ − H + Cl]$^-$, 652 [RuCl(cymene)$\mathbf{L^3}$ − 2H]$^-$, 616 [RuCl(cymene)$\mathbf{L^3}$ − HCl − 2H]$^-$, 382 [$\mathbf{L^3}$ − H]$^-$. X-ray diffraction-quality single crystals of *E*- and *Z*-**3a** could be selected directly from the reaction vessel (*E*-isomer, block-shaped; *Z*-isomer, stick-shaped).

(η^6-*p*-Cymene){9-nitro-6-[(α-picolyl-κ*N*)imino-κ*N*]-7,12-dihydroindolo[3,2-*d*][1]benzazepine}chloroosmium(II) Chloride, [OsCl(cymene)$\mathbf{L^3}$]Cl (3b). General Procedure A. Yield: 0.53 g, 66%. Anal. ($C_{32}H_{31}Cl_2N_5OOs$) C, H, N. Mp 220 °C (dec). MS (ESI+) *m/z* 744 [OsCl(cymene)$\mathbf{L^3}$]$^+$, 708 [OsCl(cymene)$\mathbf{L^3}$ − HCl]$^+$; (ESI−) *m/z* 778 [OsCl(cymene)$\mathbf{L^3}$ − H + Cl]$^-$, 742 [OsCl(cymene)$\mathbf{L^3}$ − 2H]$^-$, 706 [OsCl(cymene)$\mathbf{L^3}$ − HCl − 2H]$^-$. Single crystals of **3b** suitable for X-ray diffraction study could be selected directly from the reaction vessel.

(η^6-*p*-Cymene)[9-(pyridin-κ*N*-2-yl-(*E*)-methylidene)amino-κ*N*-7,12-dihydroindolo[3,2-*d*][1]benzazepin-6(5*H*)-one]chlororuthenium(II) Chloride, [RuCl(cymene)$\mathbf{L^4}$]Cl (4a). General Procedure B. Yield: 0.55 g, 81%. Anal. ($C_{32}H_{30}Cl_2N_4ORu$) C, H, Cl, N. Mp 280 °C (dec). MS (ESI+) *m/z* 623 [RuCl(cymene)$\mathbf{L^4}$]$^+$, 587 [RuCl(cymene)$\mathbf{L^4}$ − HCl]$^+$; (ESI−) *m/z* 657 [RuCl(cymene)$\mathbf{L^4}$ − H + Cl]$^-$, 621 [RuCl(cymene)$\mathbf{L^4}$ − 2H]$^-$, 519 [RuCl(cymene)$\mathbf{L^4}$ − cymene − 2H + MeOH]$^-$, 351 [$\mathbf{L^4}$ − H]$^-$. Single crystals suitable for X-ray diffraction study formed in a solution of **4a** in acetone at 4 °C.

(η^6-*p*-Cymene)[9-(pyridin-κ*N*-2-yl-(*E*)-methylidene)amino-κ*N*-7,12-dihydroindolo[3,2-*d*][1]benzazepin-6(5*H*)-one]chloroosmium(II) Chloride, [OsCl(cymene)$\mathbf{L^4}$]Cl (4b). General Procedure B. Yield: 0.68 g, 88%. Anal. ($C_{32}H_{30}Cl_2N_4OOs$) C, H, N. Mp 280 °C (dec). MS (ESI+) *m/z* 713 [OsCl(cymene)$\mathbf{L^4}$]$^+$, 677 [OsCl(cymene)$\mathbf{L^4}$ − HCl]$^+$; (ESI−) *m/z* 747 [OsCl(cymene)$\mathbf{L^4}$ − H + Cl]$^-$. Single crystals suitable for X-ray diffraction study formed in a solution of **4b** in acetone at 4 °C.

Acknowledgment. We thank A. Roller for the collection of X-ray data sets, C. Kowol for cyclic voltammetry measurements, and Prof. Dr. Ya. D. Lampeka for helpful discussion.

Supporting Information Available: CIF files for $\mathbf{L^3}$, *Z*-**1b**, *Z*-**2b**, *E*-**3a**, *Z*-**3a**, *E*-**3b**, **4a**, and **4b**; ORTEP views of the crystal structures of $\mathbf{L^3}$ and the cations of *Z*-**2b**, *Z*-**3b** and **4a**; time-dependent UV–vis spectra of all compounds; infrared spectra of *E*-**3a** and *Z*-**3a**; superimposed X-ray structures of the cations of *E*-**3a** and *Z*-**3a**; cyclic voltammograms of **1a**, **1b**, **4a**, and **4b**; ^{1}H NMR spectra of $\mathbf{L^1}$ and **1a**; ^{1}H NMR spectra of $\mathbf{L^3}$, *E*-**3a**, and *Z*-**3a**, 6.8−9.6 ppm; sections of the ^{1}H−^{1}H ROESY NMR spectra of *E*-**3a**, *Z*-**3a**, and **4a**; crystal data and details of data collection; selected bond distances and angles for $\mathbf{L^3}$, *E*-**3a**, *Z*-**3a**, and *E*-**3b**; cymene orientations in solution and in the solid state; ^{13}C NMR, two-dimensional spectra, and assignment; parameters of fitting data of the *E*/*Z*-isomerization to first-order kinetics; assigned ^{1}H and ^{13}C NMR shifts for all compounds; conductometric, IR, and UV–vis spectral data and elemental analyses for all compounds. This material is available free of charge via the Internet at http://pubs.acs.org.

References

(1) Guichard, S. M.; Else, R.; Reid, E.; Zeitlin, B.; Aird, R.; Muir, M.; Dodds, M.; Fiebig, H.; Sadler, P. J.; Jodrell, D. I. Anti-tumour activity in non-small cell lung cancer models and toxicity profiles for novel

ruthenium(II) based organo-metallic compounds. *Biochem. Pharmacol.* **2006**, *71*, 408–415.

(2) Ang, W. H.; Dyson, P. J. Classical and non-classical ruthenium-based anticancer drugs: towards targeted chemotherapy. *Eur. J. Inorg. Chem.* **2006**, 4003–4018.

(3) Yan, Y. K.; Melchart, M.; Habtemariam, A.; Sadler, P. J. Organometallic chemistry, biology and medicine: Ruthenium arene anticancer complexes. *Chem. Commun.* **2005**, 4764–4776.

(4) Novakova, O.; Chen, H.; Vrana, O.; Rodger, A.; Sadler, P. J. DNA interactions of monofunctional organometallic ruthenium(II) antitumor complexes in cell-free media. *Biochemistry* **2003**, *42*, 11544–11554.

(5) Deubel, D. V.; Lau, J. K.-C. In silico evolution of substrate selectivity: comparison of organometallic ruthenium complexes with the anticancer drug cisplatin. *Chem. Commun.* **2006**, 2451–2453.

(6) Liu, H.-K.; Wang, F.; Parkinson, J. A.; Bella, J.; Sadler, P. J. Ruthenation of duplex and single-stranded d(CGGCCG) by organometallic anticancer complexes. *Chem.—Eur. J.* **2006**, *12*, 6151–6165.

(7) Habtemariam, A.; Melchart, M.; Fernández, R.; Parsons, S.; Oswald, I. D. H.; Parkin, A.; Fabbiani, F. P. A.; Davidson, J. E.; Dawson, A.; Aird, R. E.; Jodrell, D. I.; Sadler, P. J. Structure-activity relationships for cytotoxic ruthenium(II) arene complexes containing N,N-, N,O-, and O,O-chelating ligands. *J. Med. Chem.* **2006**, *49*, 6858–6868.

(8) Dorcier, A.; Ang, W. H.; Bolaño, S.; Gonsalvi, L.; Juillerat-Jeannerat, L.; Laurenczy, G.; Peruzzini, M.; Phillips, A. D.; Zanobini, F.; Dyson, P. J. In vitro evaluation of rhodium and osmium RAPTA analogues: The case for organometallic anticancer drugs not based on ruthenium. *Organometallics* **2006**, *25*, 4090–4096.

(9) Dorcier, A.; Dyson, P. J.; Gossens, C.; Rothlisberger, U.; Scopelliti, R.; Tavernelli, I. Binding of organometallic ruthenium(II) and osmium(II) complexes to an oligonucleotide: a combined mass spectrometric and theoretical study. *Organometallics* **2005**, *24*, 2114–2123.

(10) Peacock, A. F. A.; Parsons, S.; Sadler, P. J. Tuning the hydrolytic aqueous chemistry of osmium arene complexes with N,O-chelating ligands to achieve cancer cell cytotoxicity. *J. Am. Chem. Soc.* **2007**, *129*, 3348–3357.

(11) Morris, R. E.; Aird, R. E.; del Socorro Murdoch, P.; Chen, H.; Cummings, J.; Hughes, N. D.; Parsons, S.; Parkin, A.; Boyd, G.; Jodrell, D. I.; Sadler, P. J. Inhibition of cancer cell growth by ruthenium(II) arene complexes. *J. Med. Chem.* **2001**, *44*, 3616–3621.

(12) Fish, R. H.; Jaouen, G. Bioorganometallic chemistry: structural diversity of organometallic complexes with bioligands and molecular recognition studies of several supramolecular hosts with biomolecules, alkali-metal ions, and organometallic pharmaceuticals. *Organometallics* **2003**, *22*, 2166–2177.

(13) Biot, C.; Glorian, G.; Maciejewski, L. A.; Brocard, J. S. Synthesis and antimalarial activity in vitro and in vivo of a new ferrocene-chloroquine analogue. *J. Med. Chem.* **1997**, *40*, 3715–3718.

(14) Debreczeni, J. É.; Bullock, A. N.; Atilla, G. E.; Williams, D. S.; Bregman, H.; Knapp, S.; Meggers, E. Ruthenium half-sandwich complexes bound to protein kinase Pim-1. *Angew. Chem., Int. Ed.* **2006**, *45*, 1580–1585.

(15) Vessières, A.; Spera, D.; Top, S.; Misterkiewicz, B.; Heldt, J.-M.; Hillard, E.; Huché, M.; Plamont, M.-A.; Napolitano, E.; Fiaschi, R.; Jaouen, G. The presence of a ferrocenyl unit on an estrogenic molecule is not always sufficient to generate in vitro cytotoxicity. *ChemMedChem.* **2006**, *1*, 1275–1281.

(16) Pellerito, C.; Nagy, L.; Pellerito, L.; Szorcsik, A. Biological activity studies on organotin(IV)$^{n+}$ complexes and parent compounds. *J. Organomet. Chem.* **2006**, *691*, 1733–1747.

(17) Vock, C. A.; Ang, W. H.; Scolaro, C.; Phillips, A. D.; Lagopoulos, L.; Juilllerat-Jeanneret, L.; Sava, G.; Scopelliti, R.; Dyson, P. J. Development of ruthenium antitumor drugs that overcome multidrug resistance mechanisms. *J. Med. Chem.* **2007**, *50*, 2166–2175.

(18) Kunick, C. Synthese von 7,12-Dihydro-indolo[3,2-*d*][1]benzazepin-6-(5*H*)-onen und 6,11-Dihydro-thieno-[3′,2′:2,3]azepino[4,5-b]indol-5(4*H*)-on. *Arch. Pharm. (Weinheim, Ger.)* **1992**, *325*, 297–299.

(19) Zaharewitz, D. W.; Gussio, R.; Leost, M.; Senderowitz, A. M.; Lahusen, T.; Kunick, C.; Meijer, L.; Sausville, E. A. Discovery and initial characterization of the paullones, a novel class of small-molecule inhibitors of cyclin-dependent kinases. *Cancer Res.* **1999**, *59*, 2566–2569.

(20) Huwe, A.; Mazitschek, R.; Giannis, A. Niedermolekulare verbindungen als inhibitoren cyclin-abhängiger kinasen. *Angew. Chem.* **2003**, *115*, 2170–2187; Small molecules as inhibitors of cyclin-dependent kinases. *Angew. Chem., Int. Ed.* **2003**, *19*, 2122–2138.

(21) Schultz, C.; Link, A.; Leost, M.; Zaharevitz, D. W.; Gussio, R.; Sausville, E. A.; Meijer, L.; Kunick, C. Paullones, a series of cyclin-dependent kinase inhibitors: Synthesis, evaluation of CDK1/cyclin B inhibition, and in vitro antitumor activity. *J. Med. Chem.* **1999**, *42*, 2909–2919.

(22) Knockaert, M.; Wieking, K.; Schmitt, S.; Leost, M.; Grant, K. M.; Mottram, J. C.; Kunick, C.; Meijer, L. Intracellular targets of paullones. Identification following affinity purification on immobilized inhibitor. *J. Biol. Chem.* **2002**, *277*, 25493–25501.

(23) Trapp, J.; Jochum, A.; Meier, R.; Saunders, L.; Marshall, B.; Kunick, C.; Verdin, E.; Goekjian, P.; Sippl, W.; Jung, M. Adenosine mimetics as inhibitors of NAD$^+$-dependent histone deacetylases, from kinase to sirtuin inhibition. *J. Med. Chem.* **2006**, *49*, 7307–7316.

(24) Hartinger, C. G.; Zorbas-Seifried, S.; Jakupec, M. A.; Kynast, B.; Zorbas, H.; Keppler, B. K. From bench to bedside—Preclinical and early clinical development of the anticancer agent indazolium *trans*-[tetrachlorobis(1*H*-indazole)ruthenate(III)] (KP1019 or FFC14A). *J. Inorg. Biochem.* **2006**, *100*, 891–904.

(25) Reisner, E.; Arion, V. B.; Guedes da Silva, M. F. C.; Lichtenecker, R.; Eichinger, A.; Keppler, B. K.; Kukushkin, V. Y.; Pombeiro, A. J. L. Tuning of redox potentials for the design of ruthenium anticancer drugs—An electrochemical study of [*trans*-$RuCl_4L(DMSO)]^-$ and [*trans*-$RuCl_4L_2]^-$ complexes, where L = imidazole, 1,2,4-triazole, indazole. *Inorg. Chem.* **2004**, *43*, 7083–7093.

(26) Lahusen, T.; De Siervi, A.; Kunick, C.; Senderowicz, A. M. Alsterpaullone, a novel cyclin-dependent kinase inhibitor, induces apoptosis by activation of caspase-9 due to perturbation in mitochondrial membrane potential. *Mol. Carcinog.* **2003**, *36*, 183–194.

(27) Kapitza, S.; Pongratz, M.; Jakupec, M. A.; Heffeter, P.; Berger, W.; Lackinger, L.; Keppler, B. K.; Marian, B. Heterocyclic complexes of ruthenium(III) induce apoptosis in colorectal carcinoma cells. *J. Cancer Res. Clin. Oncol.* **2005**, *131*, 101–110.

(28) Schmid, W. F.; Zorbas-Seifried, S.; John, R. O.; Arion, V. B.; Jakupec, M. A.; Roller, A.; Galanski, M.; Chiorescu, I.; Zorbas, H.; Keppler, B. K. The first ruthenium-based paullones: syntheses, X-ray diffraction structures, and spectroscopic and antiproliferative properties in vitro. *Inorg. Chem.* **2007**, *46*, 3645–3656.

(29) Cahn, R. S.; Ingold, C. K.; Prelog, V. Spezifikation der molekularen Chiralität. *Angew. Chem.* **1966**, *78*, 413–447; Specification of molecular chirality. *Angew. Chem., Int. Ed.* **1966**, *5*, 385–415.

(30) Lecomte, C.; Dusausoy, Y.; Protas, J.; Tirouflet, J.; Dormond, A. Structure cristalline et configuration relative d'un complexe du titanocene presentant une chiralite plane et une chiralite centree sur l'atome de titane. *J. Organomet. Chem.* **1974**, *73*, 67–76.

(31) *International Union of Pure and Applied Chemistry, Nomenclature of Inorganic Chemistry, Recommendations 2005*; The Royal Society of Chemistry: London, 2005.

(32) Dobrov, A.; Arion, V. B.; Kandler, N.; Ginzinger, W.; Jakupec, M. A.; Rufiñska, A.; Graf von Keyserlingk, N.; Galanski, M.; Kowol, C.; Keppler, B. K. The first metal-based paullone derivative with high antiproliferative activity in vitro. *Inorg. Chem.* **2006**, *45*, 1945–1950.

(33) Allen, F. A. The cambridge structural database: A quarter of a million crystal structures and rising. *Acta Crystallogr.* **2002**, *B58*, 380–388.

(34) Ciancaleoni, G.; Bellachioma, G.; Cardaci, G.; Ricci, G.; Ruzziconi, R.; Zuccaccia, D.; Macchioni, A. Cationic half-sandwich Ru(II) complexes bearing (*S*)-2-pyridyl-imino-[2.2]paracyclophane ligands: Synthesis, intramolecular, and interionic structure. *J. Organomet. Chem.* **2006**, *691*, 165–173.

(35) Peacock, A. F. A.; Habtemariam, A.; Fernández, R.; Walland, V.; Fabbiani, F. P. A.; Parsons, S.; Aird, R. E.; Jodrell, D. I.; Sadler, P. J. Tuning the reactivity of osmium(II) and ruthenium(II) arene complexes under physiological conditions. *J. Am. Chem. Soc.* **2006**, *128*, 1739–1748.

(36) Clegg, W.; Blake, A. J.; Gould, R. O.; Main, P. Crystal Structure Analysis. *International Union of Crystallography*; Oxford University Press: Oxford, U.K., 2001.

(37) The sum of the van der Waals radii of N and Cl is 1.55 + 1.75 = 3.3 Å. Radii taken from: Bondi, A. Van der Waals volumes and radii. *J. Phys. Chem.* **1964**, *68*, 441–451.

(38) Garino, C.; Ghiani, S.; Gobetto, R.; Nervi, C.; Salassa, L.; Croce, G.; Milanesio, M.; Rosenberg, E.; Ross, J. B. A. Tricarbonylchlororhenium(I) carboxaldimine derivatives: Synthesis, structure, and NMR characterization of *Z*- and *E*-isomers. *Eur. J. Inorg. Chem.* **2006**, 2885–2893.

(39) Johnson, J. E.; Morales, N. M.; Gorczyca, A. M.; Dolliver, D. D.; McAllister, M. A. Mechanisms of acid-catalyzed *Z*/*E* isomerization of imines. *J. Org. Chem.* **2001**, *66*, 7979–7985.

(40) Cunningham, I. D.; Hegarty, A. F. Acid, base, and uncatalysed isomerisation of *Z*- to *E*-amidine. A mechanistic study. *J. Chem. Soc., Perkin Trans.* **1986**, *2*, 537–541.

(41) Lauenroth, T.,Ph.D. Thesis, Hamburg University, Germany, 2001.
(42) Brunner, H. Optically active organometallic compounds of transition elements with chiral metal atoms. *Angew. Chem., Int. Ed.* **1999**, *38*, 1194–1208.
(43) Peacock, A. F. A.; Habtemariam, A.; Moggach, S. A.; Prescimone, A.; Parsons, S.; Sadler, P. J. Chloro half-sandwich osmium(II) complexes: Influence of chelated N,N-ligands on hydrolysis, guanine binding, and cytotoxicity. *Inorg. Chem.* **2007**, *46*, 4049–4059.
(44) Barette, W. C., Jr.; Johnson, H. W., Jr.; Sawyer, D. T. Voltammetric evaluation of the effective acidities (pK_a') for Broensted acids in aprotic solvents. *Anal. Chem.* **1984**, *56*, 1890–1898.
(45) Krezel, A.; Wojciech, B. A formula for correlating pK_a values determined in D_2O and H_2O. *J. Inorg. Biochem.* **2004**, *98*, 161–166.
(46) Pressprich M. R.; Chambers J. Bruker Analytical X-ray Systems. *SAINT+ Integration Engine, Program for Crystal Structure Integration*, Bruker: Madison, WI, 2004.
(47) Sheldrick, G. M., *SHELXS-97, Program for Crystal Structure Solution*, Institüt für Anorganische Chemie der Universität: Göttingen, Germany, 1997.
(48) Sheldrick, G. M., *SHELXL-97, Program for Crystal Structure Refinement*, Institüt für Anorganische Chemie der Universität: Göttingen, Germany, 1997.
(49) Johnson, G. K. *Report ORNL-5138*; OAK Ridge National Laboratory: Oak Ridge, TN, 1976.
(50) *International Tables for X-ray Crystallography*; Kluwer Academic Press: Dordrecht, The Netherlands, 1992; *Vol. C*,Tables 4.2.6.8 and 6.1.1.4.
(51) Berger, W.; Elbling, L.; Minai-Pour, M.; Vetterlein, M.; Pirker, R.; Kokoschka, E. M.; Micksche, M. Intrinsic MDR-1 gene and P-glycoprotein expression in human melanoma cell lines. *Int. J. Cancer* **1994**, *59*, 717–723.
(52) Kunick, C.; Lauenroth, K.; Wieking, K.; Xie, X.; Schultz, C.; Gussio, R.; Zaharevitz, D.; Leost, M.; Meijer, L.; Weber, A.; Jørgensen, F. S. Lemcke, T. Evaluation and comparison of 3D-QSAR CoMSIA models for CDK1, CDK5, and GSK-3 inhibition by paullones. *J. Med. Chem.* **2004**, *47*, 22–36.
(53) Bennett, M. A.; Smith, A. K. Arene ruthenium(II) complexes formed by dehydrogenation of cyclohexadienes with ruthenium(III) trichloride. *J. Chem. Soc., Dalton Trans.* **1974**, 233–241.
(54) Kiel, W. A.; Ball, G.; Graham, A. G. Carbonyl-η-hexamethylbenzene complexes of osmium. Carbon-hydrogen activation by $(\eta_6Me_6)Os(CO)(H)_2$. *J. Organomet. Chem.* **1990**, *383*, 481–496.

JM701042W